IMAGING MASS SPECTROMETRY (IMS) OF CORTICAL LIPIDS FROM PRECLINICAL TO SEVERE STAGES OF ALZHEIMER'S DISEASE

[1]Gónzalez de San Román E, [1]Manuel I, [1]Giralt MT, [2,3]Ferrer I, [1]Rodríguez-Puertas R

[1]*Department of Pharmacology, Faculty of Medicine and Nursing. University of the Basque Country (UPV/EHU), Bº Sarriena s/n, 48940 Leioa, Spain.*

[2]*Institut Neuropatologia, Servei Anatomia Patologica, IDIBELL - Hospital Universitari de Bellvitge, L'Hospitalet de Llobregat, Spain.*

[3]*Departament de Patologia i Terapèutica Experimental, Universitat de Barcelona, Barcelona, Spain*

*Corresponding author:

Rafael Rodríguez-Puertas

Department of Pharmacology. Faculty of Medicine and Nursing.

University of the Basque Country. E-48940, Leioa, Vizcaya. Spain.

E-mail: rafael.rodriguez@ehu.eus

Tel.: +34-94-6012739; fax: +34-94-6013220.

Abbreviations used in text: MALDI-IMS, Matrix Assisted Laser desorption/ionization Imaging Mass Spectrometry; AD, Alzheimer's disease; ST, sulfatide; NFT, neurofibrillary tangles; Aβ, β-amyloid; CSF, cerebrospinal fluid; BACE1, β-site APP cleavage enzyme 1; PC, phosphatidylcholine; 2-mercaptobenzothiazole (MBT); PI, Phosphatidylinositol; CPE, ceramide-1-phosphoethanolamine; CPI, ceramide-1-phosphoinositol; TIC, total ion current; PA, phosphatidic acid; SM, sphingomyelin; GlcCer,

glucosylceramide; Cer, ceramide; APP, amyloid precursor protein; APOE, apolipoprotein E ; S/N, signal/noise.

Abstract

Alzheimer's disease (AD) is a progressive neurodegenerative disease affecting millions of patients worldwide. Previous studies have demonstrated alterations in the lipid composition of lipid extracts from plasma and brain samples of AD patients. However, there is no consensus regarding the qualitative and quantitative changes of lipids in brains from AD patients. In addition, the recent developments in imaging mass spectrometry methods are leading to a new stage in the *in situ* analysis of lipid species in brain tissue slices from human *postmortem* samples. The present study uses the matrix-assisted laser desorption/ionization imaging mass spectrometry (MALDI-IMS), permitting the direct anatomical analysis of lipids in *postmortem* brain sections from AD patients, which are compared with the intensity of the lipid signal in samples from matched subjects with no neurological diseases. The frontal cortex samples from AD patients were classified in three groups based on Braak's histochemical criteria, ranging from non-cognitively impaired patients to those severely affected. The main results indicate a depletion of different sulfatide lipid species from the earliest stages of the disease in both white and gray

matter areas of the frontal cortex. Therefore, the decrease in sulfatides in cortical areas could be considered as a marker of the disease, but may also indicate neurochemical modifications related to the pathogenesis of the disease.

Keywords: Alzheimer's disease, brain, lipids, imaging mass spectrometry, frontal cortex, human.

1. Introduction

Alzheimer's disease (AD) is a progressive neurodegenerative disease affecting millions of patients worldwide. It is clinically characterized by progressive cognitive impairment, and neuropathologically, by the appearance of extracellular neuritic plaques and intraneuronal neurofibrillary tangles (NFT), together with a loss of synapses and neurons and the accumulation of lipid granules [1-3]. The neuritic plaques are largely composed of a dense amyloid core of β-amyloid (Aβ) peptide, which is generated by the amyloid precursor protein (APP) via the sequential cleavage of APP by the β-secretase (β-site APP cleavage enzyme 1; BACE1)

[reviewed in [4, 5]]. The NFT consist of a hyperphosphorylated form of the tau protein [6]. Moreover, the NFT are used as *postmortem* diagnostic criteria and also for the classification of AD patients in Braak's stages I to VI based on the severity of the disease [7].

Furthermore, there is now evidence that lipid molecules have a relevant role both in cell membrane composition and neurotransmitter signaling in different neurodegenerative diseases, such as AD. Lipid molecules could also be involved in amyloidogenesis by the regulation of APP, BACE1 and the component of γ-secretase complex, since all of them are components of lipidic bilayers [8]. The composition and organization of lipids in the cell membranes determine the trafficking properties of proteins and metabolites with important consequences in cell signaling and physiology.

On the other hand, tau is a cytoplasmic protein that stabilizes microtubules that can be modulated by lipid molecules in different ways [9-12]. Some neurodegenerative diseases such as Niemann-Pick type C is characterized by the accumulation of cholesterol and glycolipids in lysosomes, together with the presence of NFT tangles, suggesting that lipid deregulation is involved in tau pathologies [13].

The lipid composition has also been analyzed in tissue homogenates (lipid fraction) from brain samples of AD patients. Total phospholipid and sulfatide (ST) composition were found to be decreased in AD patients as compared to control subjects [14, 15][16, 17], in contrast to the increase in ceramide (Cer) and cholesterol content [16, 18]. Cer levels in the cerebrospinal fluid (CSF) were also found to be increased in

patients with AD [19], as was the level and activity of acid ceramidase in the fronto-temporal gray matter [20]. However, more recent studies described a decrease in ceramide synthase 2 activity, necessary for myelin biosynthesis, which precedes tau pathology [21]. Other changes have also been reported in the phospholipid composition of the brain, in CSF and also in plasma during different stages of AD [22-25]. A recent study analyzing more than 500 plasma samples from AD patients, reported eight phosphatidylcholine lipid species (PC) as possible biomarkers for AD and which predicted phenoconversion to either amnestic mild cognitive impairment (MCI) or to Alzheimer's disease within a 2 to 3 year timeframe, with over 90% accuracy [26].

In this context, the development of mass spectrometry during the last decade has provided us with a very useful tool not only for lipidomics, but also for the imaging of lipid species directly *in situ* with unprecedented anatomical localization, enabling the simultaneous analysis of numerous phospholipid classes using a single slice of tissue. The great potential of the new technique of matrix-assisted laser desorption/ionization imaging mass spectrometry (MALDI-IMS) in anatomical analysis has accelerated its development and applications [27-30], providing information about lipid mapping in different tissues [31]. Nevertheless, there are very few studies applying IMS to human *postmortem* brain tissue samples [32-34].

There is extensive knowledge of the biochemistry of AD, but the biochemical mechanisms underlying the pathogenesis of the disease still remain unknown, and the approved therapeutic approaches are not effective. The aim of the present study

was to find possible lipid regulations during the progression of AD in cortical areas that are affected by tau and amyloid histopathological by clearly discriminating the cortical layers from the adjacent white matter. Using MALDI-IMS we analyzed the anatomical distribution of lipids in *postmortem* human brain samples of frontal cortex (Brodmann area 8) from AD patients classified in three different groups (I-II, III-IV and V-VI) based on disease severity according to I-VI Braak's stages.

2. Materials and methods

2.1 Brain sectioning

The human brain samples were supplied by the Institute of Neuropathology (University Hospital Bellvitge, Barcelona). Human brains were obtained at autopsy after prior informed consent and with the institutional approval of the ethics committees of the University of the Basque Country (UPV/EHU), following the Code of Ethics of the World Medical Association (Declaration of Helsinki), and ensuring the privacy rights of the human subjects. The control samples were obtained from 5 males who had shown no evidence of neurological or metabolic disease. The neuropathological study disclosed no abnormalities in the brain. The AD samples were obtained from 15 males and females with AD at different Braak's stages. The intervals between death and autopsy were from 2.5 to 19 h (Table 1). Following

autopsy, the brain samples were immediately frozen at -80 ºC. The frozen tissue was brought to -20 ºC, and 20 µm thick slices were obtained in a cryostat (Microm HM55, Walldorf, Germany). Two consecutive sections were mounted on slides and kept at -25 ºC until they were treated with the chemical matrix and introduced into a MALDI metal holder (LTQ orbitrap XL).

2.2 Thionine staining

Thionine staining was performed in consecutive sections to those used in MALDI-IMS experiments to facilitate the identification of neuroanatomical structures. Tissue slices mounted onto gelatine-coated slides were hydrated after thawing. Hydration was performed by incubating tissue slices for 5 min in ethanol concentrations in a descending order (100%, 96%, 70% and 50%). Then, sections were submerged in thionine solution for 5 min. Finally, the sections were washed in deionized water and introduced in an ethanol ascendant order solution (50%, 70%, 96% and 100%) to dehydrate the tissue. The thionine stained images allowed us to delineate the area for MALDI scanning, including the six layers of the cortex and the adjacent white matter.

2.3 Sample preparation

The original lipid composition and anatomical characteristics of the tissue must be preserved throughout the sample-preparation process [35]. The frontal cortex brain samples were sectioned and stored until the moment of use, as described above.

Matrix deposition on the tissue surface was carried out by sublimation prior to analysis, using a glass sublimator (ACE glass 8023). Sublimation was performed using 300 mg of 2-mercaptobenzothiazole (MBT), which has previously been reported as being an optimal chemical matrix for phospholipid detection [36]. We controlled the deposition time and temperature (30 min, 140ºC) and the thickness of the matrix layer, which optimized the signal/noise (s/n) ratio of the mass spectra, and avoided lipid migration due to the absence of organic solvents during the sublimation procedure. Finally, a recrystallization of the sample was performed using a normal glass Petri plate (100 mm diameter x 15 mm depth), and 1 ml of methanol (99%) was added to a piece of paper previously placed in the bottom of the Petri plate in order to create a vapor atmosphere using a hot plate (1 min, 40ºC). This step allowed us to achieve higher intensities in the detection of the peaks in the mass spectra [37].

2.4 MALDI Imaging Mass Spectrometry

A MALDI LTQ-XL-Orbitrap (Thermo Fisher Scientific, Bremen, Germany) equipped with a nitrogen laser (λ = 337 nm, rep. rate = 60 Hz, spot size = 80 × 120 μm) was used for mass analysis. ImageQuest 1.0.1 software (Thermo Fisher Scientific, San Jose, CA, USA) was used for MALDI-IMS data acquisition. The images were acquired in positive ion mode in m/z range 500-1000 and in negative mode in m/z

range 400-1100, with 10 laser shots per point at laser fluence of 15 μJ. The target plate stepping distance was set to 150 μm for both the x- and y-axes by the MSI image acquisition software. The mass resolution was 100,000 (full width at half maximum as defined at *m*/*z* 400). As there may be potential displacement of the masses on the tissue due to surface irregularities and other factors, it is necessary to normalize them using the total ion current (TIC).

2.5 Image and spectra analysis of MALDI-IMS

The MALDI images were generated using ImageQuest software (Thermo Scientific, San Jose, CA). The software provided a m/z range that is plotted for signal intensity for each pixel (mass spectrum) across a given area (tissue section). The spectra normalization was performed using a ratio of the maximal peak and the mean intensity was calculated using OriginPro 8 software. The most intense peak was considered to be 100%. Differences between groups of patients were analyzed by using the Kruskal-Wallis non-parametric test followed by Dunn's post-hoc test with GraphPad Prism (San Diego, CA, USA) software. The results were considered significant when $p \leq 0.05$.

2.6 Peak Assignment

The analysis of the lipid composition of tissue samples from *postmortem* human brain used in the present study is complex. A large number of different possible lipid species were detected and some of them share similar masses and had not been detected and/or assigned to a specific lipid molecule in previous studies. Nevertheless, the assignment of lipid species was facilitated by the use of databases such as Lipid MAPS (http://www.lipidmaps.org/), Madison Metabolomics (http://mmcd.nmrfam.wisc.edu) and previous reports [38-46]. For the assignment, 5 ppm mass accuracy was selected as the tolerance window. The glycerolipid species numbers (x:y) denote the total length and the number of double bonds of the acyl chains, while the sphingolipid and sulfatide species numbers correspond to the length and number of double bonds of the acyl chain added to those of the attached sphing-4-enine (d18:1) or sphinganine (d18:0) base.

3. Results

The MALDI-IMS technique represents a useful approach to direct anatomical localization of lipids in tissue sections. In the present study this technique is applied to *postmortem* human brain sections of controls and AD patients in positive and negative ion detection mode to obtain anatomical images, which indicate the intensity of the signal for different lipid species. The results were obtained from serial sections of human brain samples of the frontal cortex area (Brodmann area 8). We compared

the data obtained from control subjects with those of AD patients classified in three groups according to different Braak's stages. The mean data for each group of patients was obtained, showing the intensity of each lipid species in both white and gray matter separately by using a specific image software, as described in the methods section, thereby clearly differentiating the lipid composition of white and gray matter. The detection of different lipid molecules, calculations and statistical analysis were carried out for the molecular ions in negative and positive mode. The analysis were carried out by setting the peak with the highest intensity at 100%, as previously explained, and normalizing the spectra as a percentage of the intensity of this maximal peak. In the case of negative ion mode in gray matter the maximal peak was the phosphatidylinositol (PI)(20:4/18:0), and in white matter it was ST (24:1). In contrast, in positive ion detection mode, the maximal peak was PC (34:1)+K^+ for both gray and white matter.

Firstly, MALDI-IMS analysis in negative ion detection mode demonstrated that ST content was reduced by more than 50% in gray matter of frontal cortex from the earliest clinically identifiable stage of AD, the group AD I-II (Figure 1, Table 2).

In contrast, in white matter, there was a decrease in all ST species from the earliest stages, which did not become statistically significant until the advanced stages of the disease, and then only for some specific ST species (Figure 2, Table 3).

Furthermore, we have observed an increase in ceramide-1-phosphoinositol (CPI) (40:2) in the earliest stages of the disease in both gray (Control 3.5 ± 0.9% vs AD I-II 20.5 ± 5.8%, $p < 0.05$) and white matter (Control 0.2 ± 0.1% vs AD I-II 6.7 ± 2.4%, p

< 0.05). However, in the most advanced stages of AD, CPI(40:2) decreased to intensities comparable with those of control subjects. In addition, another ceramide, ceramide-1-phosphoethanolamine (CPE) (38:1) was increased only in white matter from the earliest stages and reached a statistically significant increase during moderate stages of AD (Control 3.3 ± 0.8% vs. AD III-IV 8.1 ± 0.6%, $p < 0.05$). The thionine stained sections from control subjects and AD patients showed the different structures in the tissue sections and differentiated the areas of white and gray matter selected for the IMS analysis (Figure 3).

IMS method allowed us to obtain the anatomical distribution pattern of lipids in color coded images, and showed the intensity of the lipids that were modified in the cortical samples from AD patients (Figure 4 and 7). The images showed lipid intensities both in gray and white matter and the differences in lipid intensities between control subjects and AD patients in different stages of the disease. These images have been obtained by using IMS in both negative (Figure 4) and positive (Figure 7) ion detection mode.

In respect of the results obtained in positive ion mode, the levels of only a few lipid species were significantly changed in AD patients. Moreover, these lipid species do not follow a clear pattern of specific types of molecules (as was the case of the decrease in ST species in negative mode). The intensity of the signal of two lipid species was modified in cortical gray matter: phosphatidic acid (PA) (36:2)+K^+ (Control 50.9 ± 1.3% vs AD I-II 33.4 ± 3.6%, $p < 0.05$) and PA (38:2)+K^+ (Control 8.3

± 0.5 vs AD I-II 2.2 ± 0.3, $p < 0.05$). Their lowest intensities were detected in the earliest stages of AD (Figure 5, Table 4).

On the contrary, in cortical white matter we observed three lipid species with low intensities in AD patients using positive ion detection mode: PC (32:0) (Control 13.1 ± 4.2 vs AD V-VI 3.9 ± 0.5%, $p < 0.05$), sphingomyelin (SM) (d18:1/18:0) (Control 7.4 ± 1.3% vs AD III-IV 2.3 ± 0.8%, $p < 0.05$) and glucosylceramide (GlcCer) (d32:1)+K^+ (Control 18.1 ± 1.1% vs AD III-IV 10.7 ± 1.3%, $p < 0.05$) (Figure 6, Table 5).

4. Discussion

Lipid homeostasis is essential to good health and a deregulation of lipid metabolism plays an important role in many human diseases, including some neurological pathologies. In recent years, some experimental evidence indicates that impairments in some metabolic lipid pathways could be involved in the development of AD [3, 47, 48, 49]. The analysis of complex lipid mixtures through the development of soft ionization techniques (MALDI and electrospray ionization, ESI), allow us to study in greater detail these lipid pathways. The advances made in mass spectrometry technologies during recent years have given rise to the increasingly important field of lipidomics, which provides us with new opportunities to understand the metabolism and signaling by lipids in different physiological conditions and diseases [50, 51]. The present study uses IMS, to determine the involvement of changes in the lipid composition in the neurodegenerative processes, which occur in AD, and could

indicate that there is degradation of structural cell membrane molecules. Therefore, we have tried to assess the differences in lipid species in human brain samples from prefrontal cortex of AD patients at different Braak's stages (I-II, III-IV, V-VI) by using the MALDI-IMS assay. The study was performed both in positive and negative ion mode, depending on the polarity used to record the different lipid species. Usually, the phospholipid species recorded in positive ion detection mode include PA, PC and SM, and in negative mode the most common lipids detected are PE, ST, PS and PI.

The main changes we have observed in the samples from AD patients were in ST species, a class of lipid molecules that are synthesized predominantly by oligodendrocytes. These are multi-functional molecules involved in the physiology of different tissues and systems including the peripheral and central nervous systems [52-54]. In the CNS, the ST are negative regulators for the differentiation and survival of the oligodendrocytes during myelination processes [55, 56]. Studies in a ST deficient mouse model have shown the presence of structural abnormalities and loss of axonal conduction [57]. Other studies demonstrate the regulation of ST metabolism by apolipoprotein E (APOE) [42, 58], and the APOE ε4 allele is a risk factor for AD [6, 59, 60].

We report a significant reduction in different ST species in patients at different clinical stages of AD, in both cortical gray and white matter. The observed heterogeneous pattern of distribution in the obtained IMS images is characteristic for each of the molecular species within the cerebral cortex. Therefore, a precise tissue dissection is

necessary when employing other biochemical analyses, such as those using lipid extracts.

Nevertheless, as the observed ST depletion was similar in all stages of the disease, this implies that there is a ST deficiency from the onset of AD. An important conclusion, which may be drawn from our study, is that ST depletion is a metabolic impairment possibly related to synaptic dysfunction and neurodegeneration present in AD from its earliest stages. The reduction of ST in AD has previously been described by other research groups, and it has been demonstrated that this ST depletion specifically affects AD patients and does not appear in other neurodegenerative diseases, such as Parkinson's disease and Lewy body dementia [16, 17, 61]. In addition, a recent IMS study using experimental models exposed to cigarette smoke describes changes of ST species in the frontal lobe [62], thereby, supporting the possible relationship between cigarette smoking and the risk of developing AD [63]. It is important to point out that MALDI-IMS has never been used before to describe lipid changes with anatomical resolution in frontal cortex of AD patients.

The metabolic mechanisms, which produce the reduction in specific ST species observed in the frontal cortex of AD patients are still unknown. It has been suggested that an accelerated degradation of ST could lead to the production of ceramides (Cer). Some authors have reported elevated levels of Cer in AD brains compared to non-affected subjects [20, 54, 64, 65]. We observed an increase in CPI and CPE, but not in other Cer species previously reported. IMS allows anatomical detection without

purification artifacts, but the ion suppression generated by MALDI-IMS could reduce the ability to detect molecular species of low abundance [66]. Moreover, the matrix (MBT) has a molecular weight (167.25) and can produce ionization products in a mass range similar to some Cer, thereby masking their detection. It has been shown that Cer species are able to stabilize the APP cleaving enzyme 1 (BACE1), promoting Aβ biogenesis [67, 68]. On the other hand, a reduction of Cer levels leads to a reduced secretion of APP and Aβ in human neuroblastoma cells [69]. Thus, it has been suggested that Cer and Aβ could interact and induce neuronal death in AD [20]. In addition, in the APPsw transgenic mice model of familial AD, there is also ST depletion in cerebellum, but less than in cortex, supporting the idea that Aβ could be associated with ST deficiency, since Aβ accumulation does not occur to a significant extent in cerebellum [42, 70].

Different transgenic mice models have been used to analyze the relationship between ST reduction and APOE. APOE knockout mice accumulate ST in CNS, but other APOE transgenic mice harboring different APOE isoforms have shown that the modulation of ST species in CNS is APOE-isoform dependent. Moreover, in the CSF of patients without cognitive impairment who had one or two alleles of APOEε4 there was an increase in ST species when compared with those from APOEε3 subjects [71]. Therefore, it could be postulated that APOE plays an important role in the regulation of brain ST levels and serves as an extracellular ST carrier that regulates their metabolism.

In addition, it has been described that in KO mice for the lipoprotein receptor-related protein 1 (LPR1), which is related to APOE in the transport and metabolism of plasma lipids and Aβ clearance, there are deficits in brain lipid metabolism, characterized by decreased levels in cholesterol, ST and galactosylceramide. These lipid alterations positively correlate with synapse loss, neuroinflammation, memory loss and signs of neurodegeneration [72].

Due to the modifications observed when using negative ionization detection mode in AD patients, it is important to study ST lipid species during the earliest or even from prodromal stages of the disease. Specific lipid deregulation could have primary effects on the other neurodegenerative processes, including the formation of senile plaques and neurofibrillary tangles. In addition, the levels of specific ST species could be considered as biomarkers for AD.

We also observed other changes, such as the decrease of two PA in gray matter in positive ion detection mode, which is in agreement with previous studies that reported a decrease of PA in temporal gyrus of AD patients [15]. Another study demonstrated that anionic phospholipids, predominantly PA, diphosphatidyl glycerol (DPG), PS, and PI, interact with Aβ peptide, in particular with Aβ(1-43) and Aβ(1-42), increasing the fibrillization of Aβ [73, 74]. Interestingly, in our study, we found two PA species decreased in frontal cortex of AD patients, but not the DPG, PS or PI lipid species. Accordingly, in early stages of AD, cerebral PE, PI and PS were unchanged in both white and gray matter [16]. Other authors have reported a decrease in PI in temporal and occipital cortex, and in cerebellum [15, 75, 76]. All these studies used traditional

analytical techniques for phospholipid profiling, which require large brain samples and use tissue homogenates and extracts that could lead to cross contamination between different brain regions of gray and white matter. However, we minimized the sample size and the possible contamination between different brain regions, as MALDI-IMS was performed with tissue sections and gave anatomical localization of the lipids all over the tissue slice.

Finally, in this study we observed a decrease in GlcCer, SM and PC in white matter. Recent studies revealed contradictory results about SM levels in AD depending on the brain areas analyzed and on the analytical technique used. Some authors have described unchanged SM levels in CSF, and extracts from cerebellum, middle frontal gyrus white matter of frontal cortex [16, 20], whilst others have described an increase in CSF, middle frontal gyrus gray matter and cerebellum [15, 59, 76], or a decrease in SM levels in middle frontal gyrus [18]. We found that there is a decrease in one specific SM species with the progression of the disease, SM(d18:1/18:0). The oxidative stress induced by Aβ could lead to an increase in Cer levels, as described above. We observed decrease of PC (32:0), a PC with two palmitic acids in its structure, in white matter of the frontal cortex. A recent study has stated that palmitoylation of APP regulates amyloidogenic processing [77]. The lower intensities of PC (32:0) could be an indication of the release of palmitic acids and the subsequent palmitoylation of APP during the progression of the disease.

In summary, the present study shows the anatomical localization of some lipids species that are modified during the progression of the AD in frontal cortex. The identified ST species could be involved in the pathogenesis of the disease and be used as markers for AD.

A similar study of other brain areas affected by AD such as, hippocampus, nucleus basalis of Meynert and amygdala would lead to a better understanding of lipid adaptations during the progression of the disease.

5. Acknowledgements

Supported by grants from the regional Basque Government IT975-16 and ELKARTEK16/81 and Spanish Government, Ministry for Health, I. S. C. III PI 10/01202, partially financed by F.E.D.E.R.; European Union. Technical support provided by the analytical unit SGIKER (UPV/EHU, MICINN, GV, ESF) is gratefully acknowledged.

6. References

[1] D.J. Selkoe, Alzheimer's disease: genes, proteins, and therapy, Physiol. Rev. 81 (2001) 741-766.

[2] R.J. Perrin, A.M. Fagan, D.M. Holtzman, Multimodal techniques for diagnosis and prognosis of Alzheimer's disease, Nature 461 (2009) 916-922.

[3] P. Foley, Lipids in Alzheimer's disease: A century-old story, Biochim. Biophys. Acta 1801 (2010) 750-753.

[4] R.E. Tanzi, L. Bertram, Twenty years of the Alzheimer's disease amyloid hypothesis: a genetic perspective, Cell 120 (2005) 545-555.

[5] C. Haass, D.J. Selkoe, Soluble protein oligomers in neurodegeneration: lessons from the Alzheimer's amyloid beta-peptide, Nat. Rev. Mol. Cell Biol. 8 (2007) 101-112.

[6] C. Ballatore, V.M. Lee, J.Q. Trojanowski, Tau-mediated neurodegeneration in Alzheimer's disease and related disorders, Nat. Rev. Neurosci. 8 (2007) 663-672.

[7] H. Braak, E. Braak, Staging of Alzheimer's disease-related neurofibrillary changes, Neurobiol. Aging 16 (1995) 271-8; discussion 278-84.

[8] J.V. Rushworth, N.M. Hooper, Lipid Rafts: Linking Alzheimer's Amyloid-beta Production, Aggregation, and Toxicity at Neuronal Membranes, Int. J. Alzheimers Dis. 2011 (2010) 603052.

[9] G.V. Johnson, Tau phosphorylation and proteolysis: insights and perspectives, J. Alzheimers Dis. 9 (2006) 243-250.

[10] A.M. Nicholson, A. Ferreira, Increased membrane cholesterol might render mature hippocampal neurons more susceptible to beta-amyloid-induced calpain activation and tau toxicity, J. Neurosci. 29 (2009) 4640-4651.

[11] S.D. Ryan, S.N. Whitehead, L.A. Swayne, T.C. Moffat, W. Hou, M. Ethier, A.J. Bourgeois, J. Rashidian, A.P. Blanchard, P.E. Fraser, D.S. Park, D. Figeys, S.A. Bennett, Amyloid-beta42 signals tau hyperphosphorylation and compromises neuronal viability by disrupting alkylacylglycerophosphocholine metabolism, Proc. Natl. Acad. Sci. U. S. A. 106 (2009) 20936-20941.

[12] A. de Calignon, L.M. Fox, R. Pitstick, G.A. Carlson, B.J. Bacskai, T.L. Spires-Jones, B.T. Hyman, Caspase activation precedes and leads to tangles, Nature 464 (2010) 1201-1204.

[13] K. Suzuki, C.C. Parker, P.G. Pentchev, D. Katz, B. Ghetti, A.N. D'Agostino, E.D. Carstea, Neurofibrillary tangles in Niemann-Pick disease type C, Acta Neuropathol. 89 (1995) 227-238.

[14] C.G. Gottfries, B. Jungbjer, I. Karlsson, L. Svennerholm, Reductions in membrane proteins and lipids in basal ganglia of classic Alzheimer disease patients, Alzheimer Dis. Assoc. Disord. 10 (1996) 77-81.

[15] J.W. Pettegrew, K. Panchalingam, R.L. Hamilton, R.J. McClure, Brain membrane phospholipid alterations in Alzheimer's disease, Neurochem. Res. 26 (2001) 771-782.

[16] X. Han, D. M Holtzman, D.W. McKeel Jr, J. Kelley, J.C. Morris, Substantial sulfatide deficiency and ceramide elevation in very early Alzheimer's disease: potential role in disease pathogenesis, J. Neurochem. 82 (2002) 809-818.

[17] H. Cheng, J. Xu, D.W. McKeel Jr, X. Han, Specificity and potential mechanism of sulfatide deficiency in Alzheimer's disease: an electrospray ionization mass spectrometric study, Cell. Mol. Biol. (Noisy-Le-Grand) 49 (2003) 809-818.

[18] R.G. Cutler, J. Kelly, K. Storie, W.A. Pedersen, A. Tammara, K. Hatanpaa, J.C. Troncoso, M.P. Mattson, Involvement of oxidative stress-induced abnormalities in ceramide and cholesterol metabolism in brain aging and Alzheimer's disease, Proc. Natl. Acad. Sci. U. S. A. 101 (2004) 2070-2075.

[19] H. Satoi, H. Tomimoto, R. Ohtani, T. Kitano, T. Kondo, M. Watanabe, N. Oka, I. Akiguchi, S. Furuya, Y. Hirabayashi, T. Okazaki, Astroglial expression of ceramide in Alzheimer's disease brains: a role during neuronal apoptosis, Neuroscience 130 (2005) 657-666.

[20] X. He, Y. Huang, B. Li, C.X. Gong, E.H. Schuchman, Deregulation of sphingolipid metabolism in Alzheimer's disease, Neurobiol. Aging 31 (2010) 398-408.

[21] T.A. Couttas, N. Kain, A.K. Suchowerska, L.E. Quek, N. Turner, T. Fath, B. Garner, A.S. Don, Loss of ceramide synthase 2 activity, necessary for myelin biosynthesis, precedes tau pathology in the cortical pathogenesis of Alzheimer's disease, Neurobiol. Aging 43 (2016) 89-100.

[22] S.C. Cunnane, J.A. Schneider, C. Tangney, J. Tremblay-Mercier, M. Fortier, D.A. Bennett, M.C. Morris, Plasma and brain fatty acid profiles in mild cognitive impairment and Alzheimer's disease, J. Alzheimers Dis. 29 (2012) 691-697.

[23] R. Gonzalez-Dominguez, T. Garcia-Barrera, J.L. Gomez-Ariza, Combination of metabolomic and phospholipid-profiling approaches for the study of Alzheimer's disease, J. Proteomics (2014) .

[24] L. Whiley, A. Sen, J. Heaton, P. Proitsi, D. Garcia-Gomez, R. Leung, N. Smith, M. Thambisetty, I. Kloszewska, P. Mecocci, H. Soininen, M. Tsolaki, B. Vellas, S. Lovestone, C. Legido-Quigley, AddNeuroMed Consortium, Evidence of altered phosphatidylcholine metabolism in Alzheimer's disease, Neurobiol. Aging 35 (2014) 271-278.

[25] P. Chatterjee, W.L. Lim, G. Shui, V.B. Gupta, I. James, A.M. Fagan, C. Xiong, H.R. Sohrabi, K. Taddei, B.M. Brown, T. Benzinger, C. Masters, S.G. Snowden, M.R. Wenk, R.J. Bateman, J.C. Morris, R.N. Martins, Plasma Phospholipid and Sphingolipid Alterations in Presenilin1 Mutation Carriers: A Pilot Study, J. Alzheimers Dis. 50 (2015) 887-894.

[26] M. Mapstone, A.K. Cheema, M.S. Fiandaca, X. Zhong, T.R. Mhyre, L.H. Macarthur, W.J. Hall, S.G. Fisher, D.R. Peterson, J.M. Haley, M.D. Nazar, S.A. Rich, D.J. Berlau, C.B. Peltz, M.T. Tan, C.H. Kawas, H.J. Federoff, Plasma phospholipids identify antecedent memory impairment in older adults, Nat. Med. (2014) .

[27] R.M. Caprioli, T.B. Farmer, J. Gile, Molecular imaging of biological samples: localization of peptides and proteins using MALDI-TOF MS, Anal. Chem. 69 (1997) 4751-4760.

[28] P. Chaurand, M. Stoeckli, R.M. Caprioli, Direct profiling of proteins in biological tissue sections by MALDI mass spectrometry, Anal. Chem. 71 (1999) 5263-5270.

[29] M. Stoeckli, P. Chaurand, D.E. Hallahan, R.M. Caprioli, Imaging mass spectrometry: a new technology for the analysis of protein expression in mammalian tissues, Nat. Med. 7 (2001) 493-496.

[30] P.J. Todd, T.G. Schaaff, P. Chaurand, R.M. Caprioli, Organic ion imaging of biological tissue with secondary ion mass spectrometry and matrix-assisted laser desorption/ionization, J. Mass Spectrom. 36 (2001) 355-369.

[31] D. Touboul, H. Piednoel, V. Voisin, S. De La Porte, A. Brunelle, F. Halgand, O. Laprevote, Changes of phospholipid composition within the dystrophic muscle by matrix-assisted laser desorption/ionization mass spectrometry and mass spectrometry imaging, Eur. J. Mass. Spectrom. (Chichester, Eng) 10 (2004) 657-664.

[32] J. Matsumoto, Y. Sugiura, D. Yuki, T. Hayasaka, N. Goto-Inoue, N. Zaima, Y. Kunii, A. Wada, Q. Yang, K. Nishiura, H. Akatsu, A. Hori, Y. Hashizume, T. Yamamoto, K. Ikemoto, M. Setou, S. Niwa, Abnormal phospholipids distribution in the prefrontal cortex from a patient with schizophrenia revealed by matrix-assisted laser desorption/ionization imaging mass spectrometry, Anal. Bioanal Chem. 400 (2011) 1933-1943.

[33] A. Veloso, E. Astigarraga, G. Barreda-Gomez, I. Manuel, I. Ferrer, M.T. Giralt, B. Ochoa, O. Fresnedo, R. Rodriguez-Puertas, J.A. Fernandez, Anatomical distribution of lipids in human brain cortex by imaging mass spectrometry, J. Am. Soc. Mass Spectrom. 22 (2011) 329-338.

[34] A. Veloso, R. Fernandez, E. Astigarraga, G. Barreda-Gomez, I. Manuel, M.T. Giralt, I. Ferrer, B. Ochoa, R. Rodriguez-Puertas, J.A. Fernandez, Distribution of lipids in human brain, Anal. Bioanal Chem. 401 (2011) 89-101.

[35] S.A. Schwartz, M.L. Reyzer, R.M. Caprioli, Direct tissue analysis using matrix-assisted laser desorption/ionization mass spectrometry: practical aspects of sample preparation, J. Mass Spectrom. 38 (2003) 699-708.

[36] J. Yang, R.M. Caprioli, Matrix sublimation/recrystallization for imaging proteins by mass spectrometry at high spatial resolution, Anal. Chem. 83 (2011) 5728-5734.

[37] E. Astigarraga, G. Barreda-Gomez, L. Lombardero, O. Fresnedo, F. Castano, M.T. Giralt, B. Ochoa, R. Rodriguez-Puertas, J.A. Fernandez, Profiling and imaging of lipids on brain and liver tissue by matrix-assisted laser desorption/ ionization mass spectrometry using 2-mercaptobenzothiazole as a matrix, Anal. Chem. 80 (2008) 9105-9114.

[38] B. Colsch, C. Afonso, I. Popa, J. Portoukalian, F. Fournier, J.C. Tabet, N. Baumann, Characterization of the ceramide moieties of sphingoglycolipids from mouse brain by ESI-MS/MS: identification of ceramides containing sphingadienine, J. Lipid Res. 45 (2004) 281-286.

[39] J.M. Wiseman, D.R. Ifa, Q. Song, R.G. Cooks, Tissue imaging at atmospheric pressure using desorption electrospray ionization (DESI) mass spectrometry, Angew. Chem. Int. Ed Engl. 45 (2006) 7188-7192.

[40] S.N. Jackson, H.Y. Wang, A.S. Woods, In situ structural characterization of glycerophospholipids and sulfatides in brain tissue using MALDI-MS/MS, J. Am. Soc. Mass Spectrom. 18 (2007) 17-26.

[41] B. Fuchs, A. Nimptsch, R. Suss, J. Schiller, Analysis of brain lipids by directly coupled matrix-assisted laser desorption ionization time-of-flight mass spectrometry and high-performance thin-layer chromatography, J. AOAC Int. 91 (2008) 1227-1236.

[42] H. Cheng, G. Sun, K. Yang, R.W. Gross, X. Han, Selective desorption/ionization of sulfatides by MALDI-MS facilitated using 9-aminoacridine as matrix, J. Lipid Res. 51 (2010) 1599-1609.

[43] N.E. Manicke, A.L. Dill, D.R. Ifa, R.G. Cooks, High-resolution tissue imaging on an orbitrap mass spectrometer by desorption electrospray ionization mass spectrometry, J. Mass Spectrom. 45 (2010) 223-226.

[44] K. Shrivas, T. Hayasaka, N. Goto-Inoue, Y. Sugiura, N. Zaima, M. Setou, Ionic matrix for enhanced MALDI imaging mass spectrometry for identification of phospholipids in mouse liver and cerebellum tissue sections, Anal. Chem. 82 (2010) 8800-8806.

[45] K.A. Berry, J.A. Hankin, R.M. Barkley, J.M. Spraggins, R.M. Caprioli, R.C. Murphy, MALDI imaging of lipid biochemistry in tissues by mass spectrometry, Chem. Rev. 111 (2011) 6491-6512.

[46] S.N. Jackson, H.Y. Wang, A.S. Woods, Direct profiling of lipid distribution in brain tissue using MALDI-TOFMS, Anal. Chem. 77 (2005) 4523-4527.

[47] T. Hartmann, J. Kuchenbecker, M.O. Grimm, Alzheimer's disease: the lipid connection, J. Neurochem. 103 Suppl 1 (2007) 159-170.

[48] G. Di Paolo, T.W. Kim, Linking lipids to Alzheimer's disease: cholesterol and beyond, Nat. Rev. Neurosci. 12 (2011) 284-296.

[49] N. Fabelo, V. Martin, R. Marin, D. Moreno, I. Ferrer, M. Diaz, Altered lipid composition in cortical lipid rafts occurs at early stages of sporadic Alzheimer's disease and facilitates APP/BACE1 interactions, Neurobiol. Aging 35 (2014) 1801-1812.

[50] X. Han, R.W. Gross, Electrospray ionization mass spectroscopic analysis of human erythrocyte plasma membrane phospholipids, Proc. Natl. Acad. Sci. U. S. A. 91 (1994) 10635-10639.

[51] H.Y. Kim, T.C. Wang, Y.C. Ma, Liquid chromatography/mass spectrometry of phospholipids using electrospray ionization, Anal. Chem. 66 (1994) 3977-3982.

[52] J.P. Vos, M. Lopes-Cardozo, B.M. Gadella, Metabolic and functional aspects of sulfogalactolipids, Biochim. Biophys. Acta 1211 (1994) 125-149.

[53] I. Ishizuka, Chemistry and functional distribution of sulfoglycolipids, Prog. Lipid Res. 36 (1997) 245-319.

[54] T. Takahashi, T. Suzuki, Role of sulfatide in normal and pathological cells and tissues, J. Lipid Res. 53 (2012) 1437-1450.

[55] Y. Hirahara, R. Bansal, K. Honke, K. Ikenaka, Y. Wada, Sulfatide is a negative regulator of oligodendrocyte differentiation: development in sulfatide-null mice, Glia 45 (2004) 269-277.

[56] S.M. Shroff, A.D. Pomicter, W.N. Chow, M.A. Fox, R.J. Colello, S.C. Henderson, J.L. Dupree, Adult CST-null mice maintain an increased number of oligodendrocytes, J. Neurosci. Res. 87 (2009) 3403-3414.

[57] J. Marcus, S. Honigbaum, S. Shroff, K. Honke, J. Rosenbluth, J.L. Dupree, Sulfatide is essential for the maintenance of CNS myelin and axon structure, Glia 53 (2006) 372-381.

[58] X. Han, A.M. Fagan, H. Cheng, J.C. Morris, C. Xiong, D.M. Holtzman, Cerebrospinal fluid sulfatide is decreased in subjects with incipient dementia, Ann. Neurol. 54 (2003) 115-119.

[59] E.H. Corder, A.M. Saunders, W.J. Strittmatter, D.E. Schmechel, P.C. Gaskell, G.W. Small, A.D. Roses, J.L. Haines, M.A. Pericak-Vance, Gene dose of apolipoprotein E type 4 allele and the risk of Alzheimer's disease in late onset families, Science 261 (1993) 921-923.

[60] W.J. Strittmatter, K.H. Weisgraber, D.Y. Huang, L.M. Dong, G.S. Salvesen, M. Pericak-Vance, D. Schmechel, A.M. Saunders, D. Goldgaber, A.D. Roses, Binding of human apolipoprotein E to synthetic amyloid beta peptide: isoform-specific effects and implications for late-onset Alzheimer disease, Proc. Natl. Acad. Sci. U. S. A. 90 (1993) 8098-8102.

[61] H. Cheng, M. Wang, J.L. Li, N.J. Cairns, X. Han, Specific changes of sulfatide levels in individuals with pre-clinical Alzheimer's disease: an early event in disease pathogenesis, J. Neurochem. 127 (2013) 733-738.

[62] K. Nunez, J. Kay, A. Krotow, M. Tong, A.R. Agarwal, E. Cadenas, S.M. de la Monte, Cigarette Smoke-Induced Alterations in Frontal White Matter Lipid Profiles Demonstrated by MALDI-Imaging Mass Spectrometry: Relevance to Alzheimer's Disease, J. Alzheimers Dis. 51 (2016) 151-163.

[63] J.K. Cataldo, J.J. Prochaska, S.A. Glantz, Cigarette smoking is a risk factor for Alzheimer's Disease: an analysis controlling for tobacco industry affiliation, J. Alzheimers Dis. 19 (2010) 465-480.

[64] V.V. Bandaru, J. Troncoso, D. Wheeler, O. Pletnikova, J. Wang, K. Conant, N.J. Haughey, ApoE4 disrupts sterol and sphingolipid metabolism in Alzheimer's but not normal brain, Neurobiol. Aging 30 (2009) 591-599.

[65] M. Panchal, M. Gaudin, A.N. Lazar, E. Salvati, I. Rivals, S. Ayciriex, L. Dauphinot, D. Dargere, N. Auzeil, M. Masserini, O. Laprevote, C. Duyckaerts, Ceramides and sphingomyelinases in senile plaques, Neurobiol. Dis. 65 (2014) 193-201.

[66] K. Skraskova, R.M. Heeren, A review of complementary separation methods and matrix assisted laser desorption ionization-mass spectrometry imaging: lowering sample complexity, J. Chromatogr. A 1319 (2013) 1-13.

[67] S. Patil, J. Melrose, C. Chan, Involvement of astroglial ceramide in palmitic acid-induced Alzheimer-like changes in primary neurons, Eur. J. Neurosci. 26 (2007) 2131-2141.

[68] L. Puglielli, B.C. Ellis, A.J. Saunders, D.M. Kovacs, Ceramide stabilizes beta-site amyloid precursor protein-cleaving enzyme 1 and promotes amyloid beta-peptide biogenesis, J. Biol. Chem. 278 (2003) 19777-19783.

[69] I.Y. Tamboli, K. Prager, E. Barth, M. Heneka, K. Sandhoff, J. Walter, Inhibition of glycosphingolipid biosynthesis reduces secretion of the beta-amyloid precursor protein and amyloid beta-peptide, J. Biol. Chem. 280 (2005) 28110-28117.

[70] M. Gearing, J.A. Schneider, R.S. Robbins, R.D. Hollister, H. Mori, D. Games, B.T. Hyman, S.S. Mirra, Regional variation in the distribution of apolipoprotein E and A beta in Alzheimer's disease, J. Neuropathol. Exp. Neurol. 54 (1995) 833-841.

[71] X. Han, H. Cheng, J.D. Fryer, A.M. Fagan, D.M. Holtzman, Novel role for apolipoprotein E in the central nervous system. Modulation of sulfatide content, J. Biol. Chem. 278 (2003) 8043-8051.

[72] Q. Liu, J. Trotter, J. Zhang, M.M. Peters, H. Cheng, J. Bao, X. Han, E.J. Weeber, G. Bu, Neuronal LRP1 knockout in adult mice leads to impaired brain lipid metabolism and progressive, age-dependent synapse loss and neurodegeneration, J. Neurosci. 30 (2010) 17068-17078.

[73] A. Chauhan, I. Ray, V.P. Chauhan, Interaction of amyloid beta-protein with anionic phospholipids: possible involvement of Lys28 and C-terminus aliphatic amino acids, Neurochem. Res. 25 (2000) 423-429.

[74] C.E. Stokes, J.N. Hawthorne, Reduced phosphoinositide concentrations in anterior temporal cortex of Alzheimer-diseased brains, J. Neurochem. 48 (1987) 1018-1021.

[75] M.R. Prasad, M.A. Lovell, M. Yatin, H. Dhillon, W.R. Markesbery, Regional membrane phospholipid alterations in Alzheimer's disease, Neurochem. Res. 23 (1998) 81-88.

[76] M. Kosicek, H. Zetterberg, N. Andreasen, J. Peter-Katalinic, S. Hecimovic, Elevated cerebrospinal fluid sphingomyelin levels in prodromal Alzheimer's disease, Neurosci. Lett. 516 (2012) 302-305.

[77] R. Bhattacharyya, C. Barren, D.M. Kovacs, Palmitoylation of amyloid precursor protein regulates amyloidogenic processing in lipid rafts, J. Neurosci. 33 (2013) 11169-11183.

Table 1. Values are means ± SEM.

Samples	n			Age (years)	*Postmortem* (hours)
	Total	♂	♀		
Control	5	5	0	60.8 ± 4.7	6.15 ± 2.19
AD					
I-II	5	3	2	66.4 ± 3.4	6.10 ± 1.3
III-IV	5	4	1	75.8 ± 4.3	9.10 ± 2.0
V-VI	5	2	3	74.6 ± 2.0	5.45 ± 1.0

Table 2. Percentage of the relative intensity of representative lipids in gray matter of *postmortem* human frontal cortex of controls and AD patients in negative ion detection mode. The maximal peak is the most intense peak of the spectrum, in this case 885.5494 PI(20:4/18:0) which is set at 100%.

			% Intensity			
Assignment	**Cal m/z**	**Exp m/z**	**Control**	**AD I-II**	**AD III-IV**	**AD V-VI**
CPE (38:1)	715.5760	715.5735	23.5 ± 6.3	37.4 ± 6.4	35.5 ± 10.3	29.5 ± 1.5
SM (d37:1)	743.6073	743.6052	12.9 ± 2.0	13.7 ± 2.9	9.6 ± 2.5	10.6 ± 0.5
PS (18:0/18:1)	788.5442	788.5429	1.8 ± 0.9	0.5 ± 1.5	2.0 ± 1.1	1.7 ± 0.9
PE (18:0/22:6)	790.5381	790.5373	4.3 ± 1.4	3.8 ± 1.3	3.5 ± 0.7	3.9 ± 0.7
ST (d18:1/18:0)	806.5451	806.5443	1.7 ± 0.2	0.5 ± 0.2*a	0.5 ± 0.1*b	0.8 ± 0.1
PS (40:6)	834.5291	834.5282	13.6 ± 3.2	12.3 ± 2.6	13.9 ± 4.1	10.2 ± 1.2
PI (16:0/20:4)	857.5186	857.5174	9.3 ± 0.8	10.7 ± 1.0	10.5 ± 1.0	10.1 ± 0.7
ST (d18:1/h22:0)	878.6033	878.6078	6.7 ± 1.5	2.8 ± 0.8	2.6 ± 0.3*b	2.8 ± 0.7*c
PI (18:1/20:4)	883.5337	883.5320	8.5 ± 1.3	8.8 ± 1.8	7.6 ± 1.3	7.1 ± 1.1
ST (d18:1/24:1)	888.6240	888.6215	37.6 ± 4.7	18.6 ± 6.6*a	16.0 ± 2.3*b	24.0 ± 2.8
ST (d18:1/24:0)	890.6395	890.6348	8.1 ± 1.5	2.9 ± 0.9*a	3.8 ± 0.2*b	7.3 ± 0.9
ST (d18:1/h23:0) or ST (d18:0/h24:0)	892.6189	892.6352	16.5 ± 3.9	5.0 ± 1.5*a	6.4 ± 0.2	8.1 ± 1.0
CPI (40:2)+MBT	896.5779	896.5738	3.5 ± 0.9	20.5 ± 5.8*a	11.3 ± 2.8	9.7 ± 1.3
ST (d18:1/25:1) or (d18:2/25:0)	902.6396	902.6380	13.7 ± 2.0	5.3 ± 2.2	5.0 ± 0.6*b	8.3 ± 0.6
ST (d18:1/h24:1)	904.6188	904.6150	38.2 ± 7.5	16.2 ± 4.4	15.5 ± 1.3*b	17.2 ± 0.8
ST (d18:1/h24:0)	906.6345	906.6295	43.6 ± 10.3	11.6 ± 3.7*a	15.2 ± 0.5	18.4 ± 1.9
PI(18:0/22:6)	909.5488	909.5472	5.8 ± 0.8	5.1 ± 0.5	5.7 ± 0.8	5.8 ± 0.2
ST (d18:1/h25:1) or (d18:2/h25:0)	918.6346	918.6308	10.9 ± 2.1	3.8 ± 1.1*a	3.6 ± 0.4*b	5.0 ± 0.5
ST (d18:1/h25:0)	920.6502	920.6464	7.7 ± 2.2	4.9 ± 1.6	3.6 ± 1.2	5.0 ± 0.5
ST (d18:1/h26:1)	932.6502	932.6471	11.8 ± 2.7	4.7 ± 1.3	3.2 ± 0.7*b	6.1 ± 0.6

Data are mean ± SEM. The *p* values were calculated by the Kruskal-Wallis non-parametric test followed by Dunn's test. [a] AD I-II vs control, [b] AD III-IV vs control, [c]AD V-VI vs control. Control (n=5), AD I-II (n=5), AD III-IV (n=5), AD V-VI (n=5).(-): unidentified lipid species; Cal: calculated, Exp: experimental). The notation (hX:Y) denotes hydroxylated sulfatide species

Table 3. Percentage of the relative intensity of representative lipids in white matter of *postmortem* human frontal cortex of controls and AD patients in negative ion detection mode. The maximal peak is the most intense peak of the spectrum, in this case 888.6240 ST(d18:1/24:1) which is set at 100%.

			% Intensity			
Assignment	**Cal m/z**	**Exp m/z**	**Control**	**AD I-II**	**AD III-IV**	**AD V-VI**
CPE (38:1)	715.5760	715.5735	3.3 ± 0.8	7.0 ± 0.8	8.1 ± 0.6*b	6.9 ± 1.6
PS (18:0/18:1)	788.5442	788.5428	6.1 ± 2.1	9.2 ± 3.1	9.2 ± 3.7	1.7 ± 0.2
SM (d41:2)	797.6542	797.6533	3.9 ± 0.9	6.8 ± 1.3	5.2 ± 1.3	6.1 ± 0.6
ST (18:0)	806.5451	806.5443	3.7 ± 0.8	3.1 ± 0.5	2.3 ± 0.2	2.1 ± 0.2
PI (34:1)	835.5342	835.5318	2.9 ± 0.5	3.8 ± 1.4	3.9 ± 1.2	2.6 ± 0.3
PI (16:0/20:4)	857.5186	857.5165	0.7 ± 0.2	1.8 ± 1.1	0.5 ± 0.2	0.5 ± 0.3
ST (22:0)	862.6077	862.6072	2.3 ± 0.3	1.2 ± 0.5	1.2 ± 0.5	1.6 ± 0.2
ST (d18:1/h22:0)	878.6033	878.6078	6.8 ± 0.8	5.4 ± 1.3	4.3 ± 1.2	3.2 ± 0.7
PI (18:0/20:4)	885.5494	885.5473	12.1 ± 1.1	9.8 ± 1.5	10.1 ± 1.1	9.2 ± 1.6
ST (24:0)	890.6395	890.6348	29.9 ± 4.1	22.3 ± 2.1	24.0 ± 0.8	19.9 ± 2.3
ST (d18:1/23:0) or ST (d18:0/24:0)	892.6189	892.6169	15.5 ± 2.0	9.3 ± 2.1	11.5 ± 2.8	8.0 ± 2.6
CPI (40:2)+MBT	896.5779	896.5779	0.2 ± 0.1	6.7 ± 2.4*a	4.3 ± 1.6	1.8 ± 0.6
ST (d18:1/25:1) or (d18:2/25:0)	902.6396	902.6380	32.1 ± 3.0	21.3 ± 1.5*a	26.1 ± 0.6	23.2 ± 0.3
ST (d18:1/h24:1)	904.6189	904.6150	49.7 ± 5.7	35.9 ± 2.2	33.7 ± 5.7	30.8 ± 3.2*c
ST (d18:1/h24:0)	906.6345	906.6316	37.4 ± 5.0	22.8 ± 2.2	28.5 ± 4.5	20.0 ± 3.9
ST (d18:1/h25:1) or (d18:2/h25:0)	918.6346	918.6308	12.3 ± 2.0	7.2 ± 0.7	7.5 ± 0.9	6.1 ± 0.9*c
ST (d18:1/h25:0)	920.6502	920.6455	7.4 ± 1.2	4.0 ± 0.2	6.1 ± 0.5	3.7 ± 0.9*c
ST (d18:1/h26:1)	932.6502	932.6471	10.3 ± 0.8	5.3 ± 0.5*a	7.8 ± 0.4	6.7 ± 1.4

Data are mean ± SEM. The *p* values were calculated by the Kruskal-Wallis non-parametric test followed by Dunn's test. [a] AD I-II vs control, [b] AD III-IV vs control, [c]AD V-VI vs control. Control (n=5), AD I-II (n=5), AD III-IV (n=5), AD V-VI (n=5). (-) : unidentified lipid species; Cal: calculated, Exp: experimental). The notation (hX:Y) denotes hydroxylated sulfatide species.

Table 4. Percentage of the relative intensity of representative lipids in gray matter of *postmortem* human frontal cortex of controls and AD patients in positive ion detection mode. The maximal peak is the most intense peak of the spectrum, in this case 798.60 PC (34:1)+K^+ , which is set at 100%.

			% Intensity			
Assignment	**Cal m/z**	**Exp m/z**	**Control**	**AD I-II**	**AD III-IV**	**AD V-VI**
PA (34:1)+Na+	697.4779	697.4785	12.9 ± 3.4	12.6 ± 3.8	10.7 ± 2.1	10.5 ± 2.1
GlcCer (d32:1)+K+	710.4968	710.4912	20.0 ± 1.7	15.2 ± 3.2	14.9 ± 3.1	15.5 ± 0.7
PA (34:1)+K+	713.4518	713.4525	29.1 ± 1.8	20.4 ± 3.6	21.7 ± 4.0	24.3 ± 2.3
PA (36:2)+Na+	723.4935	723.4941	26.4 ± 4.9	23.8 ± 5.7	25.6 ± 3.5	22.3 ± 2.6
SM (d18:1/18:0)	731.6067	731.6083	2.7 ± 1.3	7.1 ± 0.9	7.6 ± 2.0	4.5 ± 0.6
PC (32:0)	734.5654	734.5688	18.1 ± 2.4	22.0 ± 1.6	22.7 ± 6.0	16.5 ± 3.4
PA (36:2)+K+	739.4680	739.4685	50.9 ± 1.3	33.4 ± 3.6*a	38.5 ± 4.0	40.9 ± 1.6
PA (38:2)+Na+	751.5258	751.5248	4.3 ± 1.2	2.8 ± 0.5	2.9 ± 0.3	2.8 ± 0.5
SM (d18:1/18:0)+Na+	753.5886	753.5896	20.8 ± 3.7	23.8 ± 4.9	24.2 ± 2.9	16.6 ± 2.0
PC (32:0)+Na+	756.5519	756.5534	27.4 ± 5.1	31.7 ± 5.3	27.2 ± 5.1	28.8 ± 4.6
PC (34:2)	758.5654	758.5690	2.9 ± 0.5	3.0 ± 0.5	2.9 ± 0.4	2.3 ± 0.3
PC (34:1)	760.5856	760.5858	36.9 ± 5.7	46.3 ± 7.6	48.9 ± 10.8	38.1 ± 6.3
PA (38:2)+K+	767.4988	767.5006	8.3 ± 0.5	2.2 ± 0.3*a	5.7 ± 0.4	6.1 ± 0.5
SM (d18:1/18:0)	769.5626	769.5641	15.3 ± 1.8	14.5 ± 1.4	16.4 ± 1.4	11.4 ± 1.3
PC (32:0)+k+	772.5259	772.5261	49.0 ± 4.3	54.6 ± 7.4	51.2 ± 5.1	53.3 ± 6.2
PC (34:2)+Na+	780.5519	780.5533	2.8 ± 0.3	4.3 ± 0.5	3.5 ± 0.9	3.7 ± 0.9
PC (34:1)+Na+	782.5675	782.5680	62.0 ± 10.3	67.9 ± 4.3	73.0 ± 6.3	75.8 ± 6.8
PC (36:3)	784.5856	784.5748	6.6 ± 0.9	8.8 ± 1.0	9.5 ± 1.3	7.1 ± 1.1
PC (36:1)	788.6164	788.6171	5.6 ± 1.1	6.8 ± 1.3	6.6 ± 2.1	5.3 ± 1.1
PC (34:2)+K+	796.5259	796.5261	5.2 ± 0.9	6.0 ± 0.2	5.7 ± 0.8	5.5 ± 0.5
SM (d18:1/20:0)	797.5939	797.5943	12.4 ± 1.2	11.8 ± 1.7	11.8 ± 0.6	10.3 ± 1.2
PC (36:1)+Na+	810.5988	810.5993	15.3 ± 1.8	14.5 ± 1.4	16.4 ± 1.4	11.4 ± 1.3
PC (34:6)+K+	820.5259	820.5271	7.1 ± 1.9	6.9 ± 0.7	7.4 ± 1.0	5.7 ± 0.3
PC (36:1)+K+	826.5728	826.5733	18.3 ± 0.7	16.8 ± 0.8	1 8.1 ± 1.0	15.6 ± 1.0
PC (38:4)+K+	848.5572	848.5572	6.1 ± 1.6	6.1 ± 0.7	5.9 ± 0.8	4.2 ± 0.2

Data are mean ± SEM. The *p* values were calculated by the Kruskal-Wallis non-parametric test followed by Dunn's test. [a] AD I-II vs control, [b] AD III-IV vs control, [c]AD V-VI vs control. Control (n=5), AD I-II (n=5), AD III-IV (n=5), AD V-VI (n=5). (-) : unidentified lipid species; Cal: calculated, Exp: experimental).

Table 5. Percentage of the relative intensity of representative lipids in white matter of *postmortem* human frontal cortex of controls and Alzheimer disease patients in positive ion detection mode. The maximal peak is the most intense peak of the spectrum, in this case 798.60 PC(34:1)+K^+ which is set at 100%.

			% Intensity			
Assignment	**Cal m/z**	**Exp m/z**	**Control**	**AD I-II**	**AD III-IV**	**AD V-VI**
(-)	-	610.4447	8.2 ± 2.3	3.4 ± 0.7	3.2 ± 0.2*b	3.1 ± 0.3
GlcCer (d32:1)+K+	710.4968	710.4902	18.1 ± 1.1	10.7 ± 2.1	10.7 ± 1.3*b	13.2 ± 1.1
SM (d18:1/18:0)	731.6067	731.6069	7.4 ± 1.3	4.1 ± 2.7	2.3 ± 0.8*b	3.3 ± 0.4
PC (32:0)	734.5654	734.5688	13.1 ± 4.2	6.4 ± 1.3	6.4 ± 1.5	3.9 ± 0.2*c
PA (36:2)+K+	739.4691	739.4683	49.9 ± 1.8	43.7 ± 5.6	41.9 ± 6.2	39.4 ± 1.8
PA (38:2)+Na+	751.5258	751.5248	4.9 ± 2.1	6.6 ± 0.8	4.9 ± 0.9	4.5 ± 0.6
SM (d18:1/18:0)+Na+	753.5886	753.5889	15.8 ± 3.4	14.6 ± 2.9	16.2 ± 3.6	12.3 ± 1.9
PC (32:0)+Na+	756.5519	756.5522	5.8 ± 0.5	7.3 ± 1.6	5.2 ± 1.6	6.5 ± 0.6
PC (34:1)	760.5856	760.5856	47.5 ± 11.2	56.6 ± 14.3	24.2 ± 2.9	35.5 ± 4.2
PA (38:2)+K+	767.4988	767.5004	15.1 ± 1.4	14.0 ± 2.6	38.6 ± 5.6	10.5 ± 1.9
SM (d18:1/18:0)+K+	769.5626	769.5629	30.1 ± 2.0	24.8 ± 2.3	1.5 ± 2.4	26.9 ± 1.2
PC (32:0)+K+	772.5259	772.5271	17.8 ± 2.2	15.5 ± 1.3	25.3 ± 2.2	10.6 ± 1.4*c
(-)	-	776.5951	13.7 ± 4.1	12.5 ± 2.3	12.2 ± 1.3	10.5 ± 1.3
PC (34:1)+Na+	782.5675	782.5691	43.9 ± 9.4	61.0 ± 8.8	9.0 ± 1.8	49.7 ± 7.0
PC (36:3)	784.5856	784.5743	6.7 ± 1.2	7.1 ± 1.1	61.0 ± 9.1	5.6 ± 0.5
PC (36:1)	788.6157	788.6195	18.0 ± 2.8	18.3 ± 4.8	6.6 ± 0.7	9.2 ± 0.5
(-)	-	792.5689	13.9 ± 0.9	11.3 ± 2.6	11.9 ± 3.9	17.1 ± 2.6
PC (34:2)+K+	796.5259	796.5248	4.7 ± 0.6	5.2 ± 0.1	9.7 ± 1.5	5.0 ± 0.7
PC (38:5)	808.5851	808.5844	8.4 ± 2.6	10.0 ± 1.7	4.8 ± 0.5	7.6 ± 1.3
PC (36:1)+Na+	810.5988	810.6004	21.7 ± 3.9	20.7 ± 2.9	8.6 ± 2.4	14.1 ± 0.7
PC (36:2)+K+	824.5571	824.5576	14.5 ± 1.2	15.9 ± 0.6	1.6 ± 3.7	15.4 ± 1.5
PC (36:1)+K+	826.5728	826.5757	34.5 ± 0.9	35.7 ± 3.5	3.7 ± 2.8	25.1 ± 1.6
SM (42:2)+Na+	835.6663	835.6684	19.5 ± 3.7	16.0 ± 2.7	30.5 ± 4.6	15.8 ± 1.5
SM (42:2)+K+	851.6403	851.6411	30.9 ± 1.8	23.5 ± 2.6	4.3 ± 2.5	29.2 ± 3.4

Data are mean ± SEM. The *p* values were calculated by the Kruskal-Wallis non-parametric test followed by Dunn's test. [a] AD I-II vs control, [b] AD III-IV vs control, [c]AD V-VI vs control. Control (n=5), AD I-II (n=5), AD III-IV (n=5), AD V-VI (n=5). (-): unidentified lipid species; Cal: calculated, Exp: experimental).

Legends:

Figure 1. Average spectra comparison between controls and AD patients. Mass spectra were obtained from the average spectra recorded directly from the tissue slice, selecting only the gray matter from the frontal cortex of the tissue slices. The spectra parameters were obtained using 2 micro scans/step with 10 laser shots and a raster step size of 150 µm with the laser power at 15-20 µJ and using MBT matrix. Detection was performed in negative ion mode. The "y" axis represents the intensity of the measured MS signal as a percentage of the maximal peak. The maximal peak is the most intense peak of the spectrum, in this case 885.5494 PI (20:4/18:0) which is set at 100%.

Figure 2. Comparison of average mass spectra from controls (n=5) and AD patients, obtained from the average spectra recorded directly from the tissue slice, selecting only white matter. The spectra parameters were 2 micro scans/step with 10 laser shots and a raster step size of 150 µm with the laser power at 15-20 µJ and using MBT matrix. Detection is performed in negative ion mode. The "y" axis represents the intensity of the measured MS signal as percentage of the maximal peak. The maximal peak is the most intense peak in this case 888.6254 ST (18:0/20:4) of the spectrum, which is set at 100%.

Figure 3. Representative images of thionine stained brain sections of control (A), AD I-II (B), AD III-IV (C), AD V-VI (D). Bar: 1 cm.

Figure 4. The image shows the distribution of representative lipid species that were found to be modified when controls were compared with AD patients at different stages of the disease. The color-coded images show areas of gray and white matter in the frontal cortex of human brain tissue. The spectra were recorded with 150 µm spacing. Ten shots were accumulated at each point with the spectrometer working in negative ion mode. Laser power was set at 15-20 µJ.

Figure 5. Average mass spectra in positive ion mode from control subjects and AD patients selecting only gray matter. The spectra parameters were 2 micro scans/step with 10 laser shots and a raster step size of 150 µm with the laser power at 15-20 µJ and using MBT matrix. The "y" axis represents the intensity of the measured MS signal as percentage of the maximal peak. The maximal peak is the most intense peak of the spectrum, in this case 798.60 PC (34:1)+K^+, which is set at 100%.

Figure 6. Average mass spectra in positive ionization detection mode corresponding to the control group and the three groups of AD patients that were obtained selecting only white matter. The spectra parameters were 2 micro scans/step with 10 laser shots and a raster step size of 150 µm with the laser power at 15-20µJ and using MBT matrix. The "y" axis represents the intensity of the measured MS signal as percentage of the maximal peak. The maximal peak is the most intense peak of the spectrum in this case 798.60 PC (34:1)+K^+, which is set at 100%.

Figure 7. The image shows the distribution of some representative lipid species that were found modified in gray or white matter areas of the frontal cortex from human brain tissue (controls and AD patients at three different stages of the disease). The spectra were recorded with 150 µm spacing. Ten shots were accumulated at each point with the spectrometer working in positive ion mode. Laser power was set at 15-20 µJ.

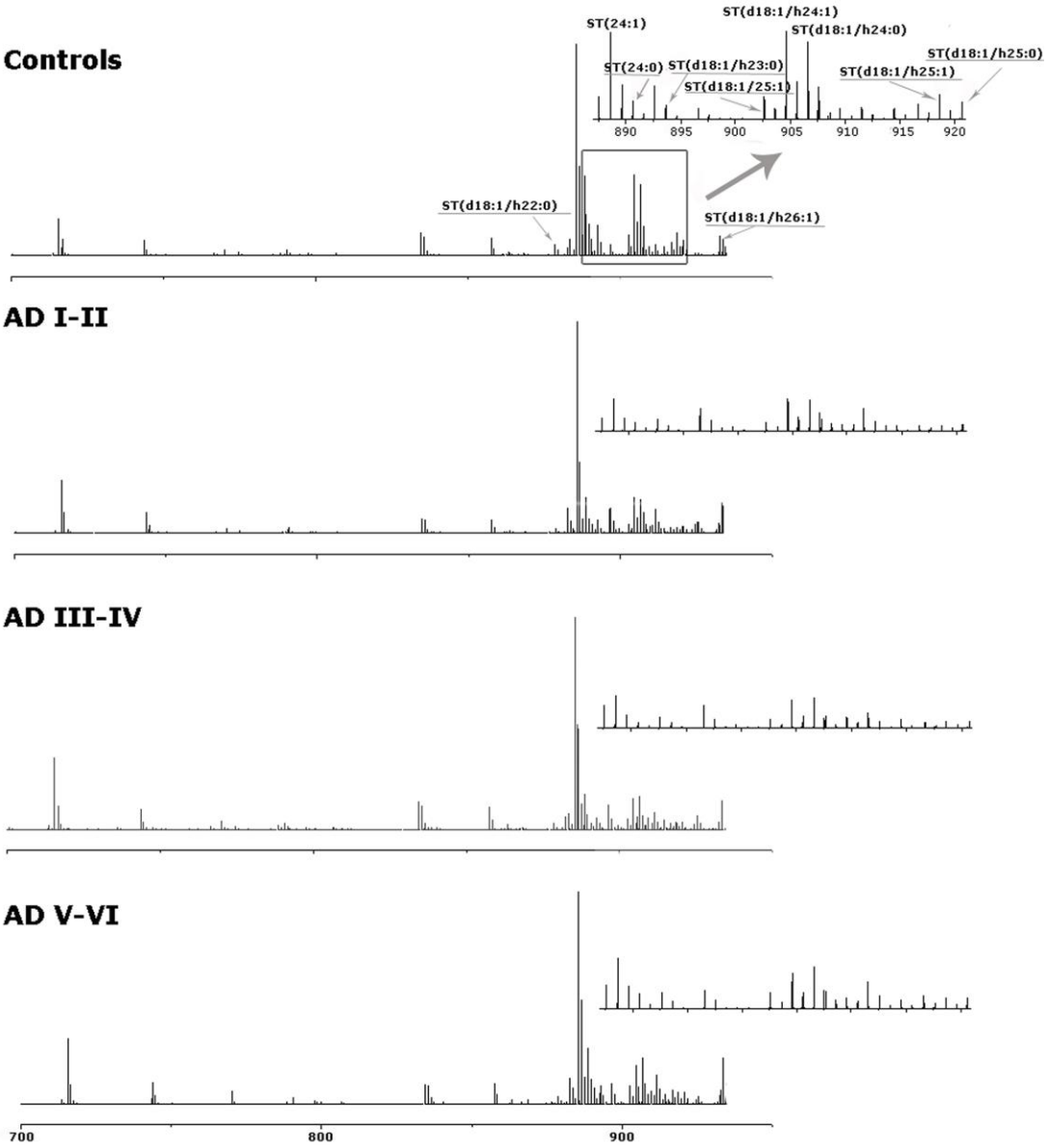
Controls
ST(24:1)
ST(d18:1/h24:1)
ST(d18:1/h24:0)
ST(d18:1/h25:0)
ST(24:0)
ST(d18:1/h23:0)
ST(d18:1/25:1)
ST(d18:1/h25:1)
890
895
900
905
910
915
920
ST(d18:1/h22:0)
ST(d18:1/h26:1)
AD I-II
AD III-IV
AD V-VI
700
800
900

Figure 1.

Figure 2.

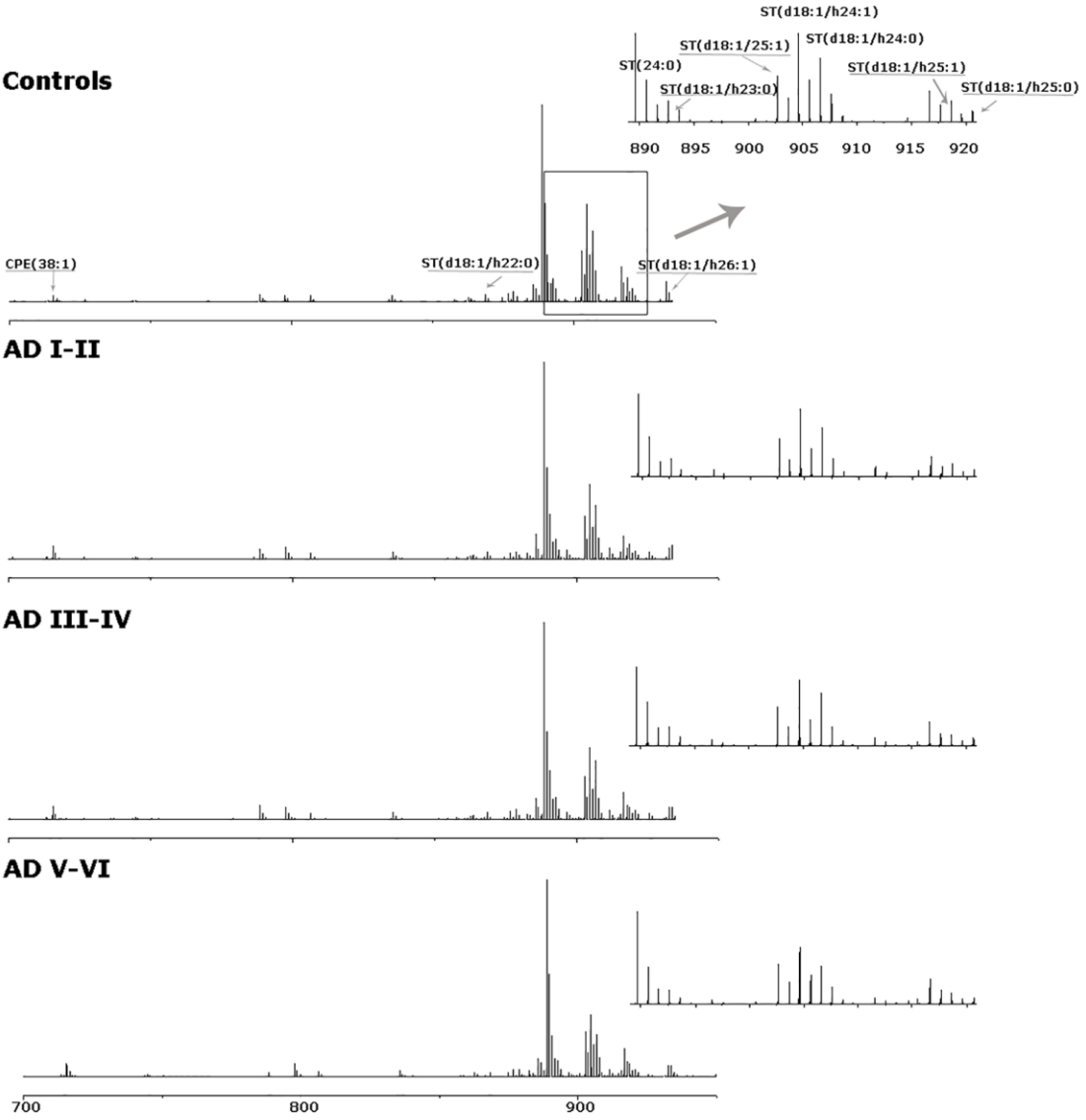
Controls
ST(d18:1/h24:1)
ST(d18:1/25:1)
ST(d18:1/h24:0)
ST(24:0)
ST(d18:1/h25:1)
ST(d18:1/h23:0)
ST(d18:1/h25:0)
890
895
900
905
910
915
920
CPE(38:1)
ST(d18:1/h22:0)
ST(d18:1/h26:1)
AD I-II
AD III-IV
AD V-VI
700
800
900

Figure 3.

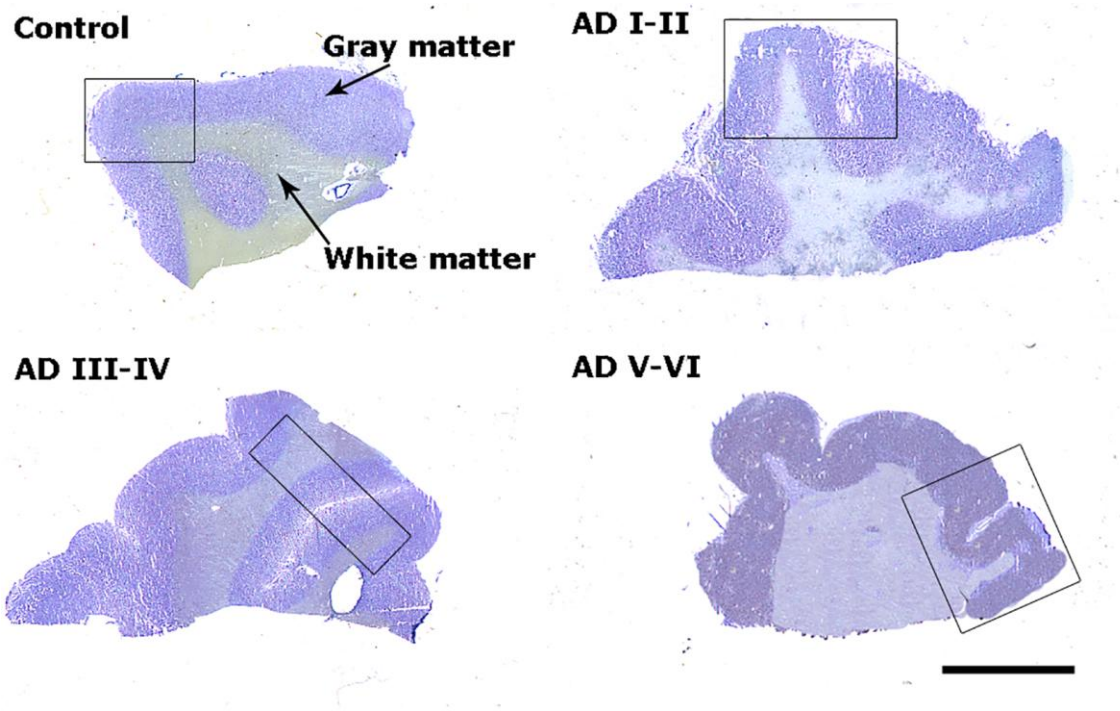

Figure 4.

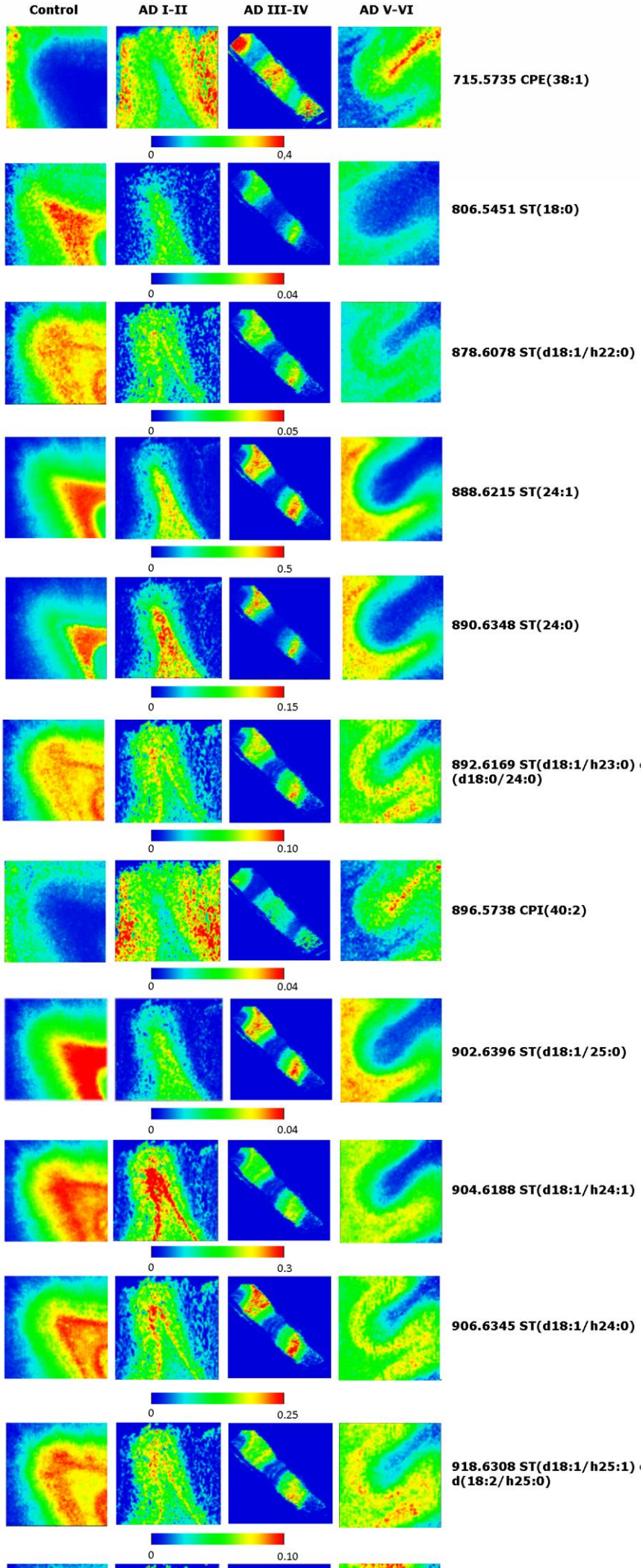
Control
AD I-II
AD III-IV
AD V-VI
715.5735 CPE(38:1)
0
0,4
806.5451 ST(18:0)
0
0.04
878.6078 ST(d18:1/h22:0)
0
0.05
888.6215 ST(24:1)
0
0.5
890.6348 ST(24:0)
0
0.15
892.6169 ST(d18:1/h23:0)
(d18:0/24:0)
0
0.10
896.5738 CPI(40:2)
0
0.04
902.6396 ST(d18:1/25:0)
0
0.04
904.6188 ST(d18:1/h24:1)
0
0.3
906.6345 ST(d18:1/h24:0)
0
0.25
918.6308 ST(d18:1/h25:1)
d(18:2/h25:0)
0
0.10

Figure 5.

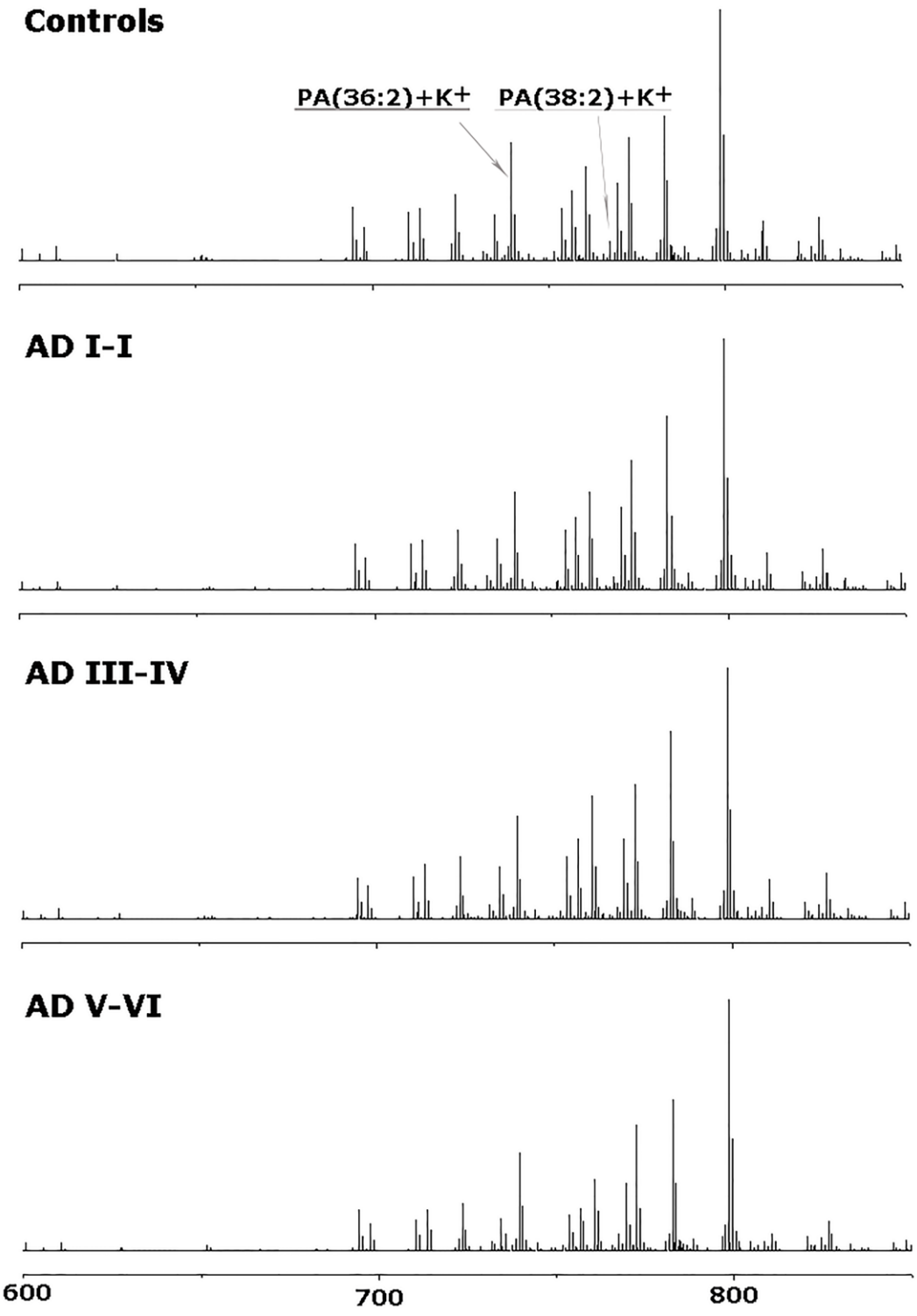

Figure 6.

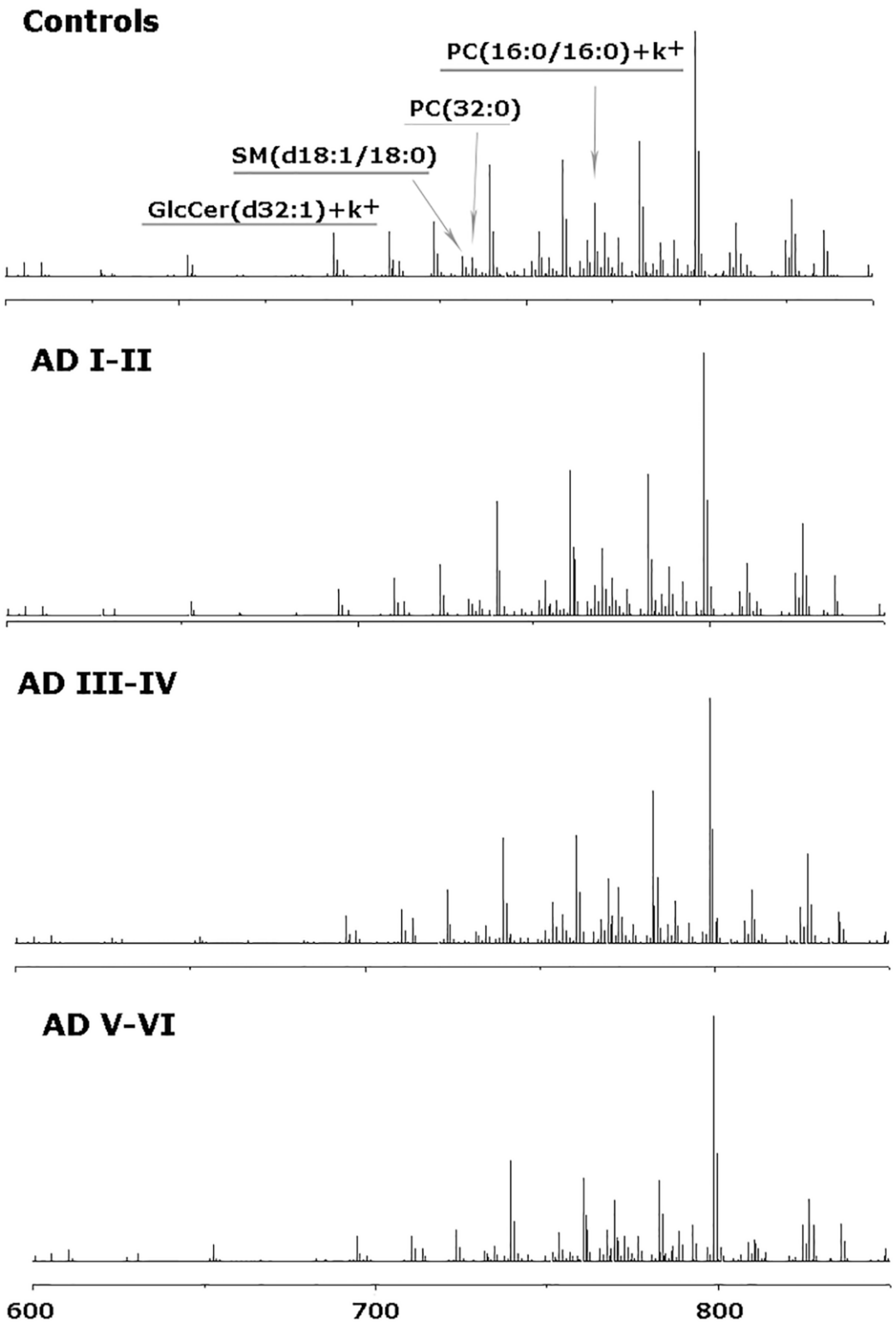
Controls
PC(16:0/16:0)+k+
PC(32:0)
SM(d18:1/18:0)
GlcCer(d32:1)+k+
AD I-II
AD III-IV
AD V-VI
600
700
800

Figure 7.

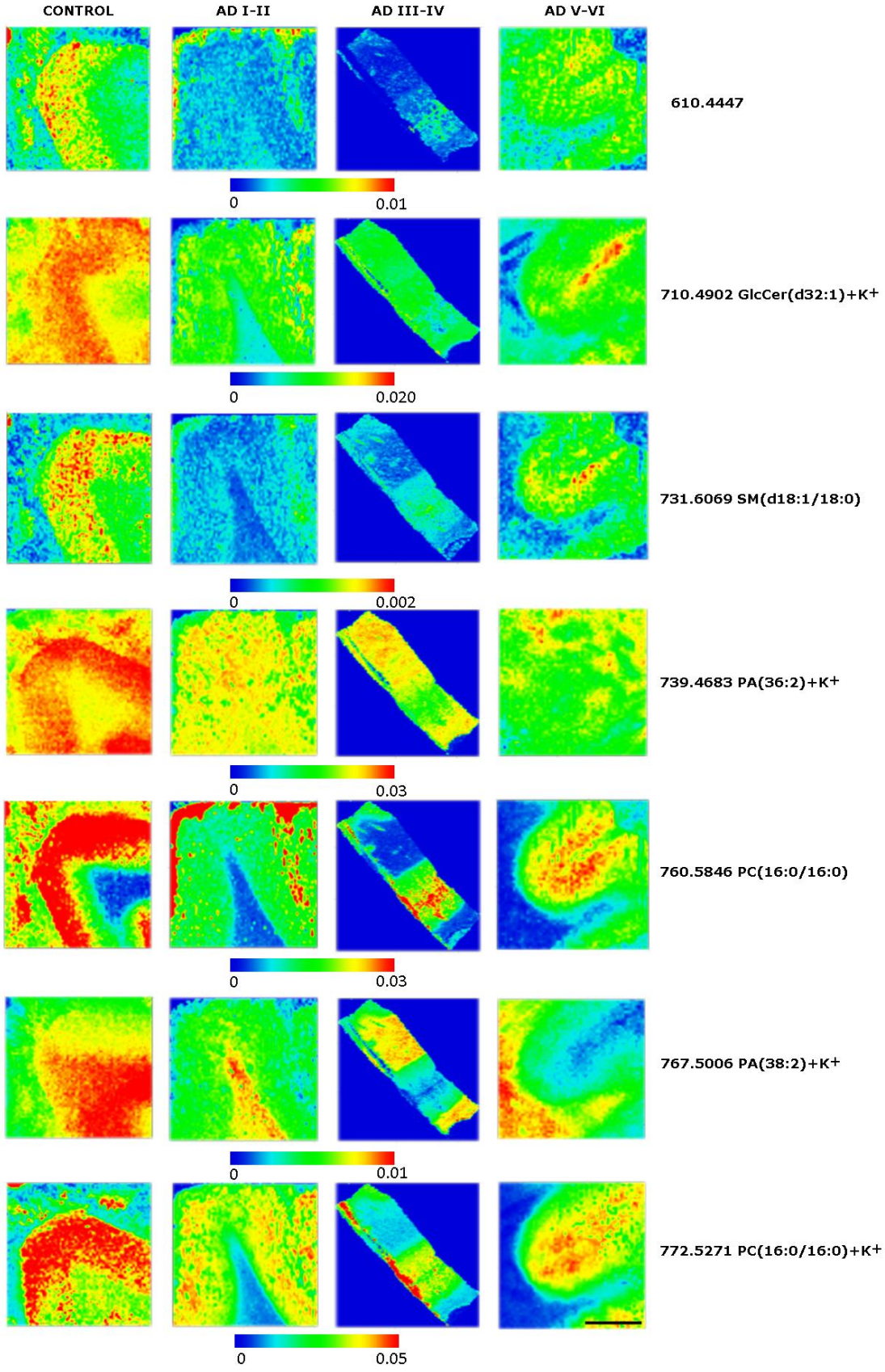
CONTROL
AD I-II
AD III-IV
AD V-VI
610.4447
0
0.01
710.4902 GlcCer(d32:1)+K+
0
0.020
731.6069 SM(d18:1/18:0)
0
0.002
739.4683 PA(36:2)+K+
0
0.03
760.5846 PC(16:0/16:0)
0
0.03
767.5006 PA(38:2)+K+
0
0.01
772.5271 PC(16:0/16:0)+K+
0
0.05

Graphical abstract.

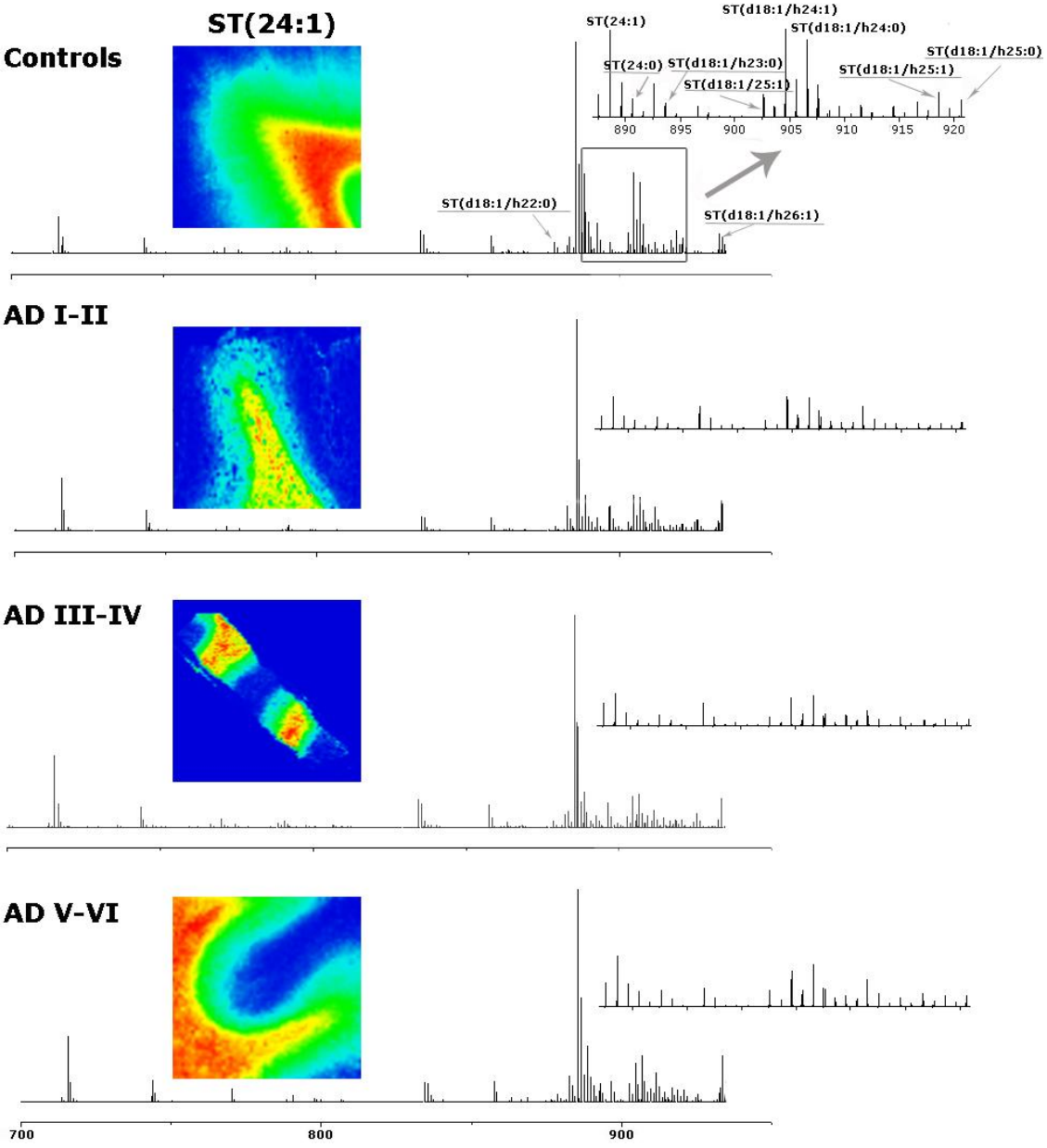

Highlights

- Lipid imaging mass spectrometry in AD patients shows several changes in different lipid species between AD and age-matched control patients.
- High decrease of ST species in AD patients compared with age-matched controls.
- ST decrease could be related with axon deregulation leading to synaptic dysfunction.

Tables

Table 1. Values are means ± SEM.

	n				
		♂	♀		*Postmortem*
Samples	**Total**			**Age (years)**	**(hours)**
Control	5	5	0	60.8 ± 4.7	6.15 ± 2.19
AD					
I-II	5	3	2	66.4 ± 3.4	6.10 ± 1.3
III-IV	5	4	1	75.8 ± 4.3	9.10 ± 2.0
V-VI	5	2	3	74.6 ± 2.0	5.45 ± 1.0

Table 2. Percentage of the relative intensity of representative lipids in gray matter of *postmortem* human frontal cortex of controls and AD patients in negative ion detection mode. The maximal peak is the most intense peak of the spectrum, in this case 885.5494 PI(20:4/18:0) which is set at 100%.

			% Intensity			
Assignment	**Cal m/z**	**Exp m/z**	**Control**	**AD I-II**	**AD III-IV**	**AD V-VI**
CPE (38:1)	715.5760	715.5735	23.5 ± 6.3	37.4 ± 6.4	35.5 ± 10.3	29.5 ± 1.5
SM (d37:1)	743.6073	743.6052	12.9 ± 2.0	13.7 ± 2.9	9.6 ± 2.5	10.6 ± 0.5
PS (18:0/18:1)	788.5442	788.5429	1.8 ± 0.9	0.5 ± 1.5	2.0 ± 1.1	1.7 ± 0.9
PE (18:0/22:6)	790.5381	790.5373	4.3 ± 1.4	3.8 ± 1.3	3.5 ± 0.7	3.9 ± 0.7
ST (d18:1/18:0)	806.5451	806.5443	1.7 ± 0.2	0.5 ± 0.2*a	0.5 ± 0.1*b	0.8 ± 0.1
PS (40:6)	834.5291	834.5282	13.6 ± 3.2	12.3 ± 2.6	13.9 ± 4.1	10.2 ± 1.2
PI (16:0/20:4)	857.5186	857.5174	9.3 ± 0.8	10.7 ± 1.0	10.5 ± 1.0	10.1 ± 0.7
ST (d18:1/h22:0)	878.6033	878.6078	6.7 ± 1.5	2.8 ± 0.8	2.6 ± 0.3*b	2.8 ± 0.7*c
PI (18:1/20:4)	883.5337	883.5320	8.5 ± 1.3	8.8 ± 1.8	7.6 ± 1.3	7.1 ± 1.1
ST (d18:1/24:1)	888.6240	888.6215	37.6 ± 4.7	18.6 ± 6.6*a	16.0 ± 2.3*b	24.0 ± 2.8
ST (d18:1/24:0)	890.6395	890.6348	8.1 ± 1.5	2.9 ± 0.9*a	3.8 ± 0.2*b	7.3 ± 0.9
ST (d18:1/h23:0) or ST (d18:0/h24:0)	892.6189	892.6352	16.5 ± 3.9	5.0 ± 1.5*a	6.4 ± 0.2	8.1 ± 1.0
CPI (40:2)+MBT	896.5779	896.5738	3.5 ± 0.9	20.5 ± 5.8*a	11.3 ± 2.8	9.7 ± 1.3
ST (d18:1/25:1) or (d18:2/25:0)	902.6396	902.6380	13.7 ± 2.0	5.3 ± 2.2	5.0 ± 0.6*b	8.3 ± 0.6
ST (d18:1/h24:1)	904.6188	904.6150	38.2 ± 7.5	16.2 ± 4.4	15.5 ± 1.3*b	17.2 ± 0.8
ST (d18:1/h24:0)	906.6345	906.6295	43.6 ± 10.3	11.6 ± 3.7*a	15.2 ± 0.5	18.4 ± 1.9
PI(18:0/22:6)	909.5488	909.5472	5.8 ± 0.8	5.1 ± 0.5	5.7 ± 0.8	5.8 ± 0.2
ST (d18:1/h25:1) or (d18:2/h25:0)	918.6346	918.6308	10.9 ± 2.1	3.8 ± 1.1*a	3.6 ± 0.4*b	5.0 ± 0.5
ST (d18:1/h25:0)	920.6502	920.6464	7.7 ± 2.2	4.9 ± 1.6	3.6 ± 1.2	5.0 ± 0.5
ST (d18:1/h26:1)	932.6502	932.6471	11.8 ± 2.7	4.7 ± 1.3	3.2 ± 0.7*b	6.1 ± 0.6

Data are mean ± SEM. The *p* values were calculated by the Kruskal-Wallis non-parametric test followed by Dunn's test. [a] AD I-II vs control, [b] AD III-IV vs control, [c]AD V-VI vs control. Control (n=5), AD I-II (n=5), AD III-IV (n=5), AD V-VI (n=5).(-): unidentified lipid species; Cal: calculated, Exp: experimental). The notation (hX:Y) denotes hydroxylated sulfatide species

Table 3. Percentage of the relative intensity of representative lipids in white matter of *postmortem* human frontal cortex of controls and AD patients in negative ion detection mode. The maximal peak is the most intense peak of the spectrum, in this case 888.6240 ST(d18:1/24:1) which is set at 100%.

			% Intensity			
Assignment	**Cal m/z**	**Exp m/z**	**Control**	**AD I-II**	**AD III-IV**	**AD V-VI**
CPE (38:1)	715.5760	715.5735	3.3 ± 0.8	7.0 ± 0.8	8.1 ± 0.6*b	6.9 ± 1.6
PS (18:0/18:1)	788.5442	788.5428	6.1 ± 2.1	9.2 ± 3.1	9.2 ± 3.7	1.7 ± 0.2
SM (d41:2)	797.6542	797.6533	3.9 ± 0.9	6.8 ± 1.3	5.2 ± 1.3	6.1 ± 0.6
ST (18:0)	806.5451	806.5443	3.7 ± 0.8	3.1 ± 0.5	2.3 ± 0.2	2.1 ± 0.2
PI (34:1)	835.5342	835.5318	2.9 ± 0.5	3.8 ± 1.4	3.9 ± 1.2	2.6 ± 0.3
PI (16:0/20:4)	857.5186	857.5165	0.7 ± 0.2	1.8 ± 1.1	0.5 ± 0.2	0.5 ± 0.3
ST (22:0)	862.6077	862.6072	2.3 ± 0.3	1.2 ± 0.5	1.2 ± 0.5	1.6 ± 0.2
ST (d18:1/h22:0)	878.6033	878.6078	6.8 ± 0.8	5.4 ± 1.3	4.3 ± 1.2	3.2 ± 0.7
PI (18:0/20:4)	885.5494	885.5473	12.1 ± 1.1	9.8 ± 1.5	10.1 ± 1.1	9.2 ± 1.6
ST (24:0)	890.6395	890.6348	29.9 ± 4.1	22.3 ± 2.1	24.0 ± 0.8	19.9 ± 2.3
ST (d18:1/23:0) or ST (d18:0/24:0)	892.6189	892.6169	15.5 ± 2.0	9.3 ± 2.1	11.5 ± 2.8	8.0 ± 2.6
CPI (40:2)+MBT	896.5779	896.5779	0.2 ± 0.1	6.7 ± 2.4*a	4.3 ± 1.6	1.8 ± 0.6
ST (d18:1/25:1) or (d18:2/25:0)	902.6396	902.6380	32.1 ± 3.0	21.3 ± 1.5*a	26.1 ± 0.6	23.2 ± 0.3
ST (d18:1/h24:1)	904.6189	904.6150	49.7 ± 5.7	35.9 ± 2.2	33.7 ± 5.7	30.8 ± 3.2*c
ST (d18:1/h24:0)	906.6345	906.6316	37.4 ± 5.0	22.8 ± 2.2	28.5 ± 4.5	20.0 ± 3.9
ST (d18:1/h25:1) or (d18:2/h25:0)	918.6346	918.6308	12.3 ± 2.0	7.2 ± 0.7	7.5 ± 0.9	6.1 ± 0.9*c
ST (d18:1/h25:0)	920.6502	920.6455	7.4 ± 1.2	4.0 ± 0.2	6.1 ± 0.5	3.7 ± 0.9*c
ST (d18:1/h26:1)	932.6502	932.6471	10.3 ± 0.8	5.3 ± 0.5*a	7.8 ± 0.4	6.7 ± 1.4

Data are mean ± SEM. The *p* values were calculated by the Kruskal-Wallis non-parametric test followed by Dunn's test. [a] AD I-II vs control, [b] AD III-IV vs control, [c]AD V-VI vs control. Control (n=5), AD I-II (n=5), AD III-IV (n=5), AD V-VI (n=5). (-) : unidentified lipid species; Cal: calculated, Exp: experimental). The notation (hX:Y) denotes hydroxylated sulfatide species.

Table 4. Percentage of the relative intensity of representative lipids in gray matter of *postmortem* human frontal cortex of controls and AD patients in positive ion detection mode. The maximal peak is the most intense peak of the spectrum, in this case 798.60 PC (34:1)+K^+ , which is set at 100%.

			% Intensity			
Assignment	**Cal m/z**	**Exp m/z**	**Control**	**AD I-II**	**AD III-IV**	**AD V-VI**
PA (34:1)+Na+	697.4779	697.4785	12.9 ± 3.4	12.6 ± 3.8	10.7 ± 2.1	10.5 ± 2.1
GlcCer (d32:1)+K+	710.4968	710.4912	20.0 ± 1.7	15.2 ± 3.2	14.9 ± 3.1	15.5 ± 0.7
PA (34:1)+K+	713.4518	713.4525	29.1 ± 1.8	20.4 ± 3.6	21.7 ± 4.0	24.3 ± 2.3
PA (36:2)+Na+	723.4935	723.4941	26.4 ± 4.9	23.8 ± 5.7	25.6 ± 3.5	22.3 ± 2.6
SM (d18:1/18:0)	731.6067	731.6083	2.7 ± 1.3	7.1 ± 0.9	7.6 ± 2.0	4.5 ± 0.6
PC (32:0)	734.5654	734.5688	18.1 ± 2.4	22.0 ± 1.6	22.7 ± 6.0	16.5 ± 3.4
PA (36:2)+K+	739.4680	739.4685	50.9 ± 1.3	33.4 ± 3.6*a	38.5 ± 4.0	40.9 ± 1.6
PA (38:2)+Na+	751.5258	751.5248	4.3 ± 1.2	2.8 ± 0.5	2.9 ± 0.3	2.8 ± 0.5
SM (d18:1/18:0)+Na+	753.5886	753.5896	20.8 ± 3.7	23.8 ± 4.9	24.2 ± 2.9	16.6 ± 2.0
PC (32:0)+Na+	756.5519	756.5534	27.4 ± 5.1	31.7 ± 5.3	27.2 ± 5.1	28.8 ± 4.6
PC (34:2)	758.5654	758.5690	2.9 ± 0.5	3.0 ± 0.5	2.9 ± 0.4	2.3 ± 0.3
PC (34:1)	760.5856	760.5858	36.9 ± 5.7	46.3 ± 7.6	48.9 ± 10.8	38.1 ± 6.3
PA (38:2)+K+	767.4988	767.5006	8.3 ± 0.5	2.2 ± 0.3*a	5.7 ± 0.4	6.1 ± 0.5
SM (d18:1/18:0)	769.5626	769.5641	15.3 ± 1.8	14.5 ± 1.4	16.4 ± 1.4	11.4 ± 1.3
PC (32:0)+k+	772.5259	772.5261	49.0 ± 4.3	54.6 ± 7.4	51.2 ± 5.1	53.3 ± 6.2
PC (34:2)+Na+	780.5519	780.5533	2.8 ± 0.3	4.3 ± 0.5	3.5 ± 0.9	3.7 ± 0.9
PC (34:1)+Na+	782.5675	782.5680	62.0 ± 10.3	67.9 ± 4.3	73.0 ± 6.3	75.8 ± 6.8
PC (36:3)	784.5856	784.5748	6.6 ± 0.9	8.8 ± 1.0	9.5 ± 1.3	7.1 ± 1.1
PC (36:1)	788.6164	788.6171	5.6 ± 1.1	6.8 ± 1.3	6.6 ± 2.1	5.3 ± 1.1
PC (34:2)+K+	796.5259	796.5261	5.2 ± 0.9	6.0 ± 0.2	5.7 ± 0.8	5.5 ± 0.5
SM (d18:1/20:0)	797.5939	797.5943	12.4 ± 1.2	11.8 ± 1.7	11.8 ± 0.6	10.3 ± 1.2
PC (36:1)+Na+	810.5988	810.5993	15.3 ± 1.8	14.5 ± 1.4	16.4 ± 1.4	11.4 ± 1.3
PC (34:6)+K+	820.5259	820.5271	7.1 ± 1.9	6.9 ± 0.7	7.4 ± 1.0	5.7 ± 0.3
PC (36:1)+K+	826.5728	826.5733	18.3 ± 0.7	16.8 ± 0.8	1 8.1 ± 1.0	15.6 ± 1.0
PC (38:4)+K+	848.5572	848.5572	6.1 ± 1.6	6.1 ± 0.7	5.9 ± 0.8	4.2 ± 0.2

Data are mean ± SEM. The *p* values were calculated by the Kruskal-Wallis non-parametric test followed by Dunn's test. [a] AD I-II vs control, [b] AD III-IV vs control, [c]AD V-VI vs control. Control (n=5), AD I-II (n=5), AD III-IV (n=5), AD V-VI (n=5). (-) : unidentified lipid species; Cal: calculated, Exp: experimental).

Table 5. Percentage of the relative intensity of representative lipids in white matter of *postmortem* human frontal cortex of controls and Alzheimer disease patients in positive ion detection mode. The maximal peak is the most intense peak of the spectrum, in this case 798.60 PC(34:1)+K^+ which is set at 100%.

			% Intensity			
Assignment	**Cal m/z**	**Exp m/z**	**Control**	**AD I-II**	**AD III-IV**	**AD V-VI**
(-)	-	610.4447	8.2 ± 2.3	3.4 ± 0.7	3.2 ± 0.2*b	3.1 ± 0.3
GlcCer (d32:1)+K+	710.4968	710.4902	18.1 ± 1.1	10.7 ± 2.1	10.7 ± 1.3*b	13.2 ± 1.1
SM (d18:1/18:0)	731.6067	731.6069	7.4 ± 1.3	4.1 ± 2.7	2.3 ± 0.8*b	3.3 ± 0.4
PC (32:0)	734.5654	734.5688	13.1 ± 4.2	6.4 ± 1.3	6.4 ± 1.5	3.9 ± 0.2*c
PA (36:2)+K+	739.4691	739.4683	49.9 ± 1.8	43.7 ± 5.6	41.9 ± 6.2	39.4 ± 1.8
PA (38:2)+Na+	751.5258	751.5248	4.9 ± 2.1	6.6 ± 0.8	4.9 ± 0.9	4.5 ± 0.6
SM (d18:1/18:0)+Na+	753.5886	753.5889	15.8 ± 3.4	14.6 ± 2.9	16.2 ± 3.6	12.3 ± 1.9
PC (32:0)+Na+	756.5519	756.5522	5.8 ± 0.5	7.3 ± 1.6	5.2 ± 1.6	6.5 ± 0.6
PC (34:1)	760.5856	760.5856	47.5 ± 11.2	56.6 ± 14.3	24.2 ± 2.9	35.5 ± 4.2
PA (38:2)+K+	767.4988	767.5004	15.1 ± 1.4	14.0 ± 2.6	38.6 ± 5.6	10.5 ± 1.9
SM (d18:1/18:0)+K+	769.5626	769.5629	30.1 ± 2.0	24.8 ± 2.3	1.5 ± 2.4	26.9 ± 1.2
PC (32:0)+K+	772.5259	772.5271	17.8 ± 2.2	15.5 ± 1.3	25.3 ± 2.2	10.6 ± 1.4*c
(-)	-	776.5951	13.7 ± 4.1	12.5 ± 2.3	12.2 ± 1.3	10.5 ± 1.3
PC (34:1)+Na+	782.5675	782.5691	43.9 ± 9.4	61.0 ± 8.8	9.0 ± 1.8	49.7 ± 7.0
PC (36:3)	784.5856	784.5743	6.7 ± 1.2	7.1 ± 1.1	61.0 ± 9.1	5.6 ± 0.5
PC (36:1)	788.6157	788.6195	18.0 ± 2.8	18.3 ± 4.8	6.6 ± 0.7	9.2 ± 0.5
(-)	-	792.5689	13.9 ± 0.9	11.3 ± 2.6	11.9 ± 3.9	17.1 ± 2.6
PC (34:2)+K+	796.5259	796.5248	4.7 ± 0.6	5.2 ± 0.1	9.7 ± 1.5	5.0 ± 0.7
PC (38:5)	808.5851	808.5844	8.4 ± 2.6	10.0 ± 1.7	4.8 ± 0.5	7.6 ± 1.3
PC (36:1)+Na+	810.5988	810.6004	21.7 ± 3.9	20.7 ± 2.9	8.6 ± 2.4	14.1 ± 0.7
PC (36:2)+K+	824.5571	824.5576	14.5 ± 1.2	15.9 ± 0.6	1.6 ± 3.7	15.4 ± 1.5
PC (36:1)+K+	826.5728	826.5757	34.5 ± 0.9	35.7 ± 3.5	3.7 ± 2.8	25.1 ± 1.6
SM (42:2)+Na+	835.6663	835.6684	19.5 ± 3.7	16.0 ± 2.7	30.5 ± 4.6	15.8 ± 1.5
SM (42:2)+K+	851.6403	851.6411	30.9 ± 1.8	23.5 ± 2.6	4.3 ± 2.5	29.2 ± 3.4

Data are mean ± SEM. The *p* values were calculated by the Kruskal-Wallis non-parametric test followed by Dunn's test. [a] AD I-II vs control, [b] AD III-IV vs control, [c]AD V-VI vs control. Control (n=5), AD I-II (n=5), AD III-IV (n=5), AD V-VI (n=5). (-): unidentified lipid species; Cal: calculated, Exp: experimental).

Figure 1

Click here to download high resolution image

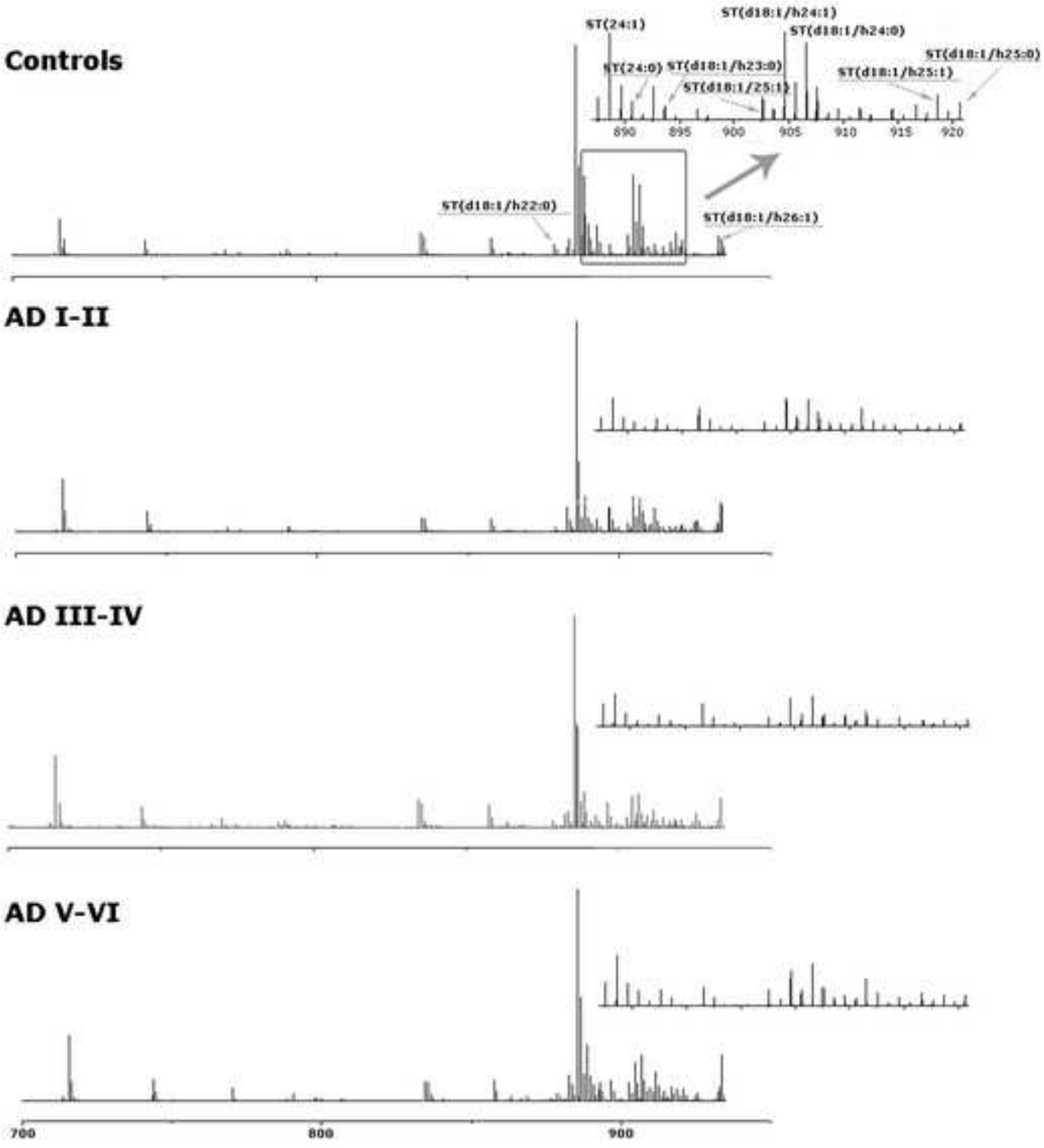

Figure 2

Click here to download high resolution image

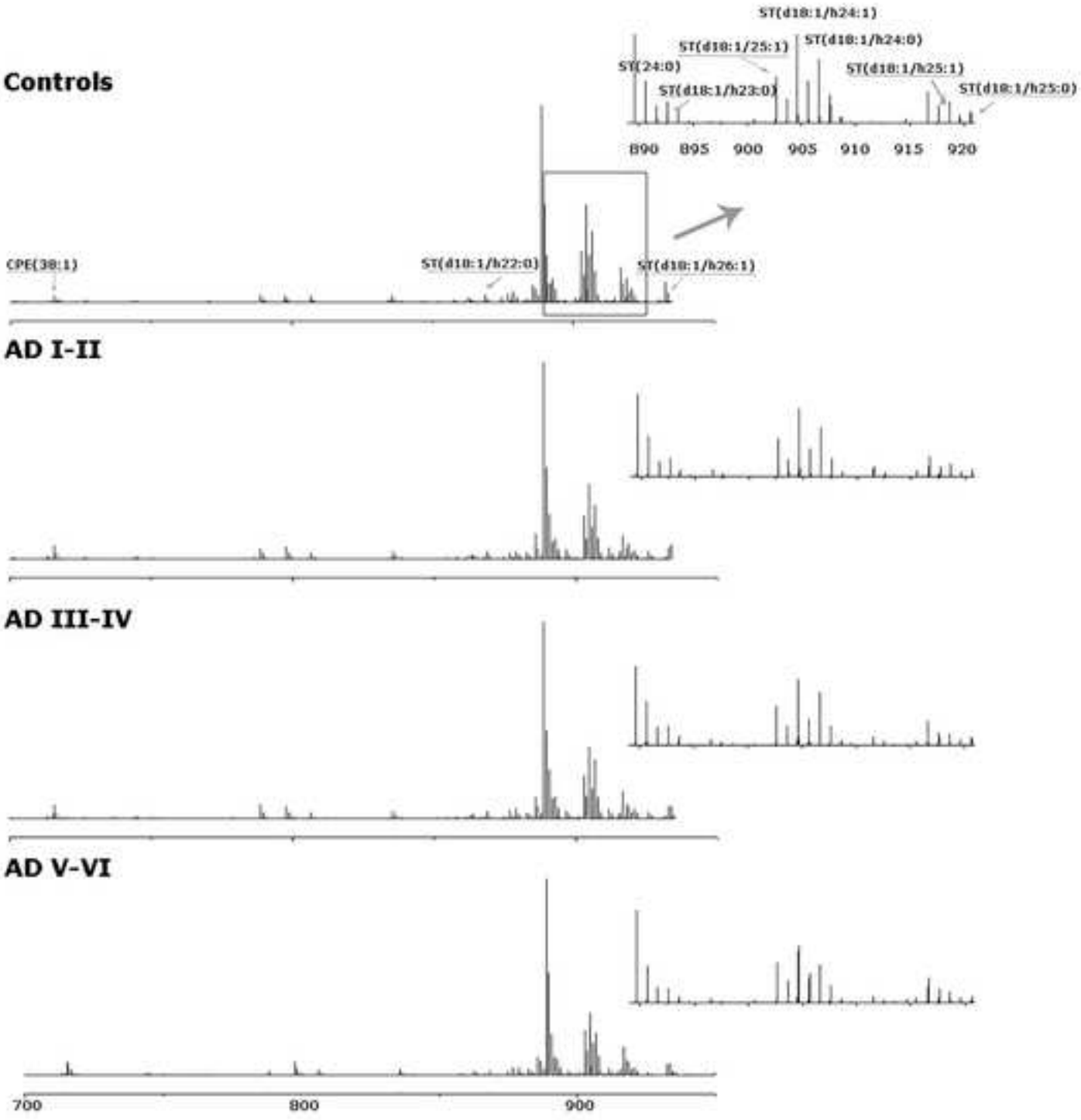

Figure 3

Click here to download high resolution image

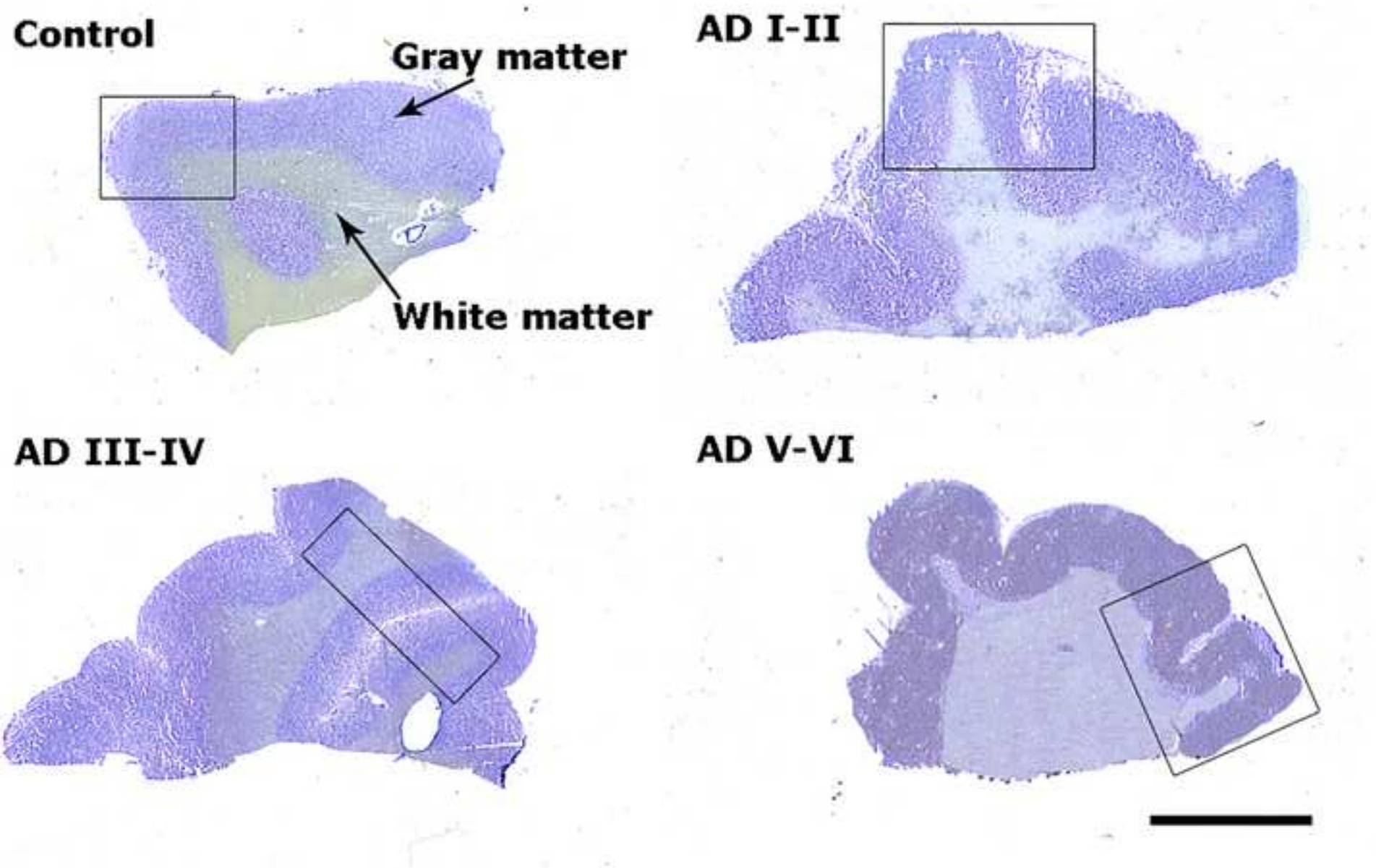

Figure 4

Click here to download high resolution image

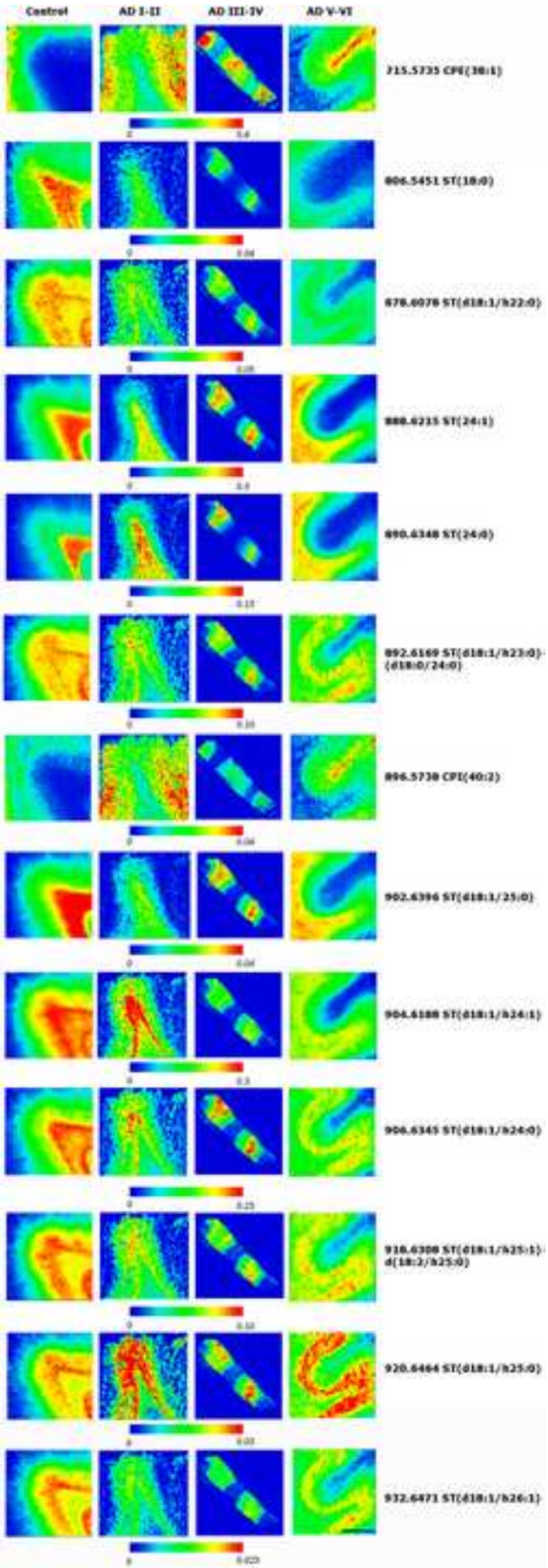

Figure 5

Click here to download high resolution image

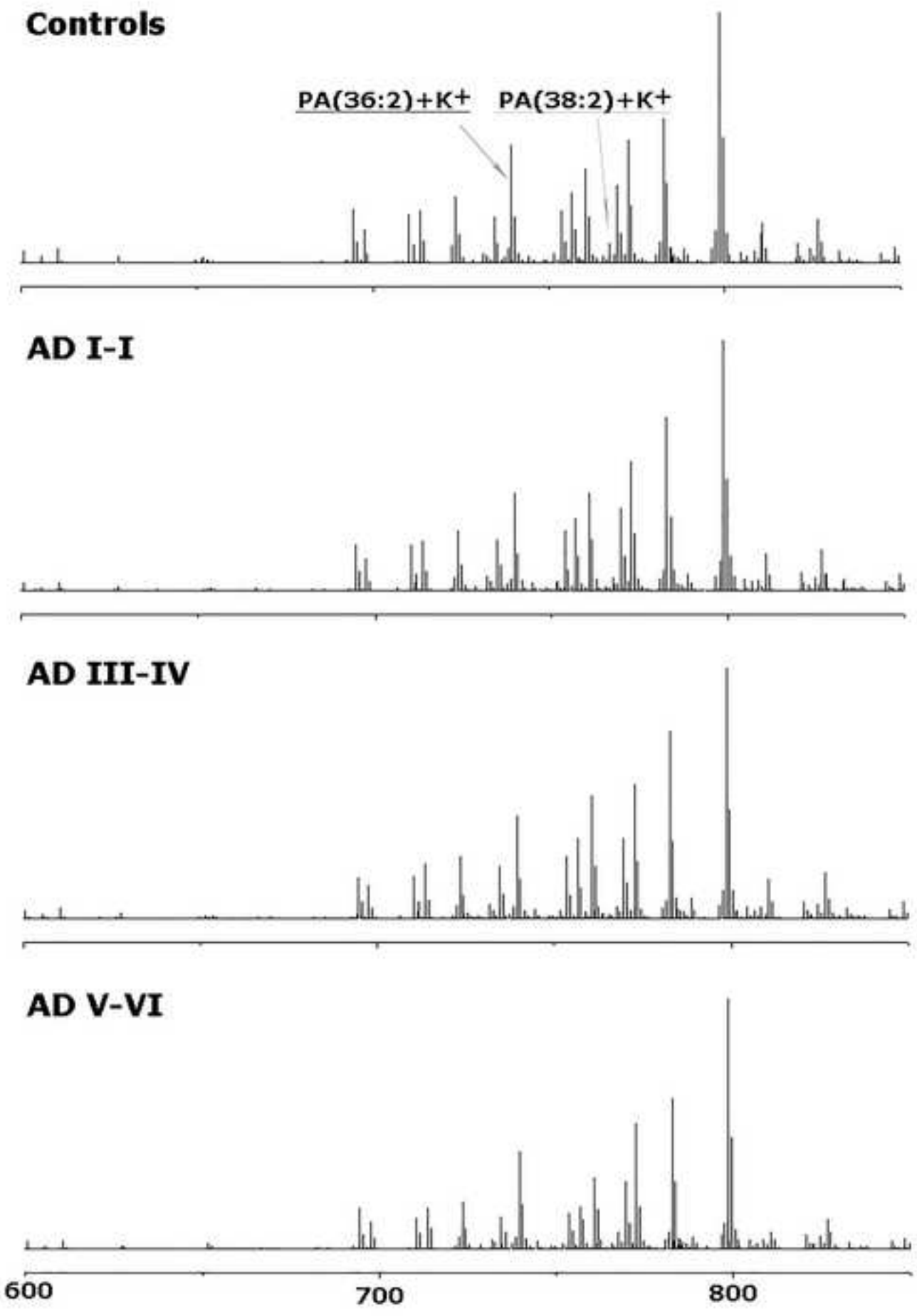

Figure 6

Click here to download high resolution image

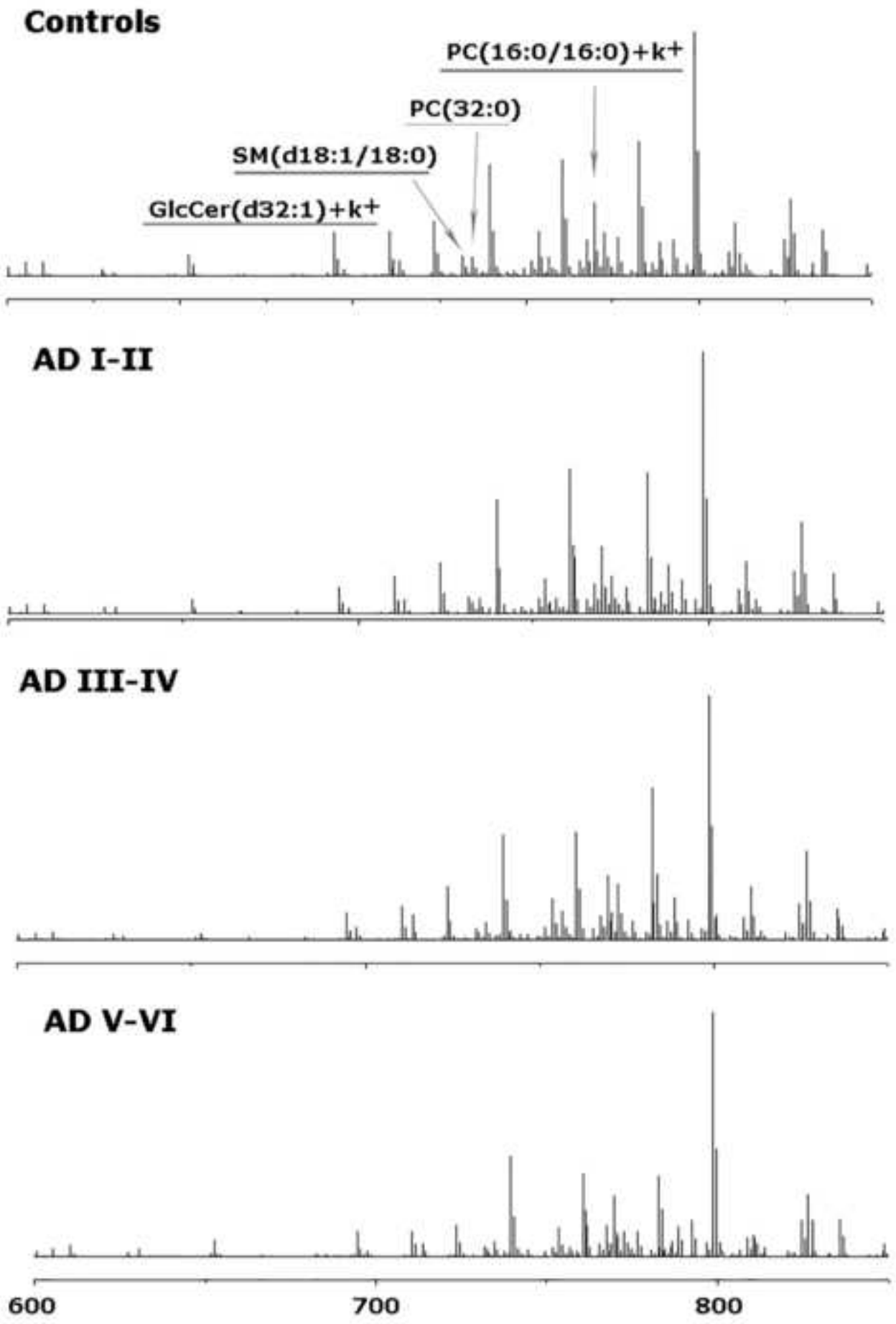

Figure 7

Click here to download high resolution image

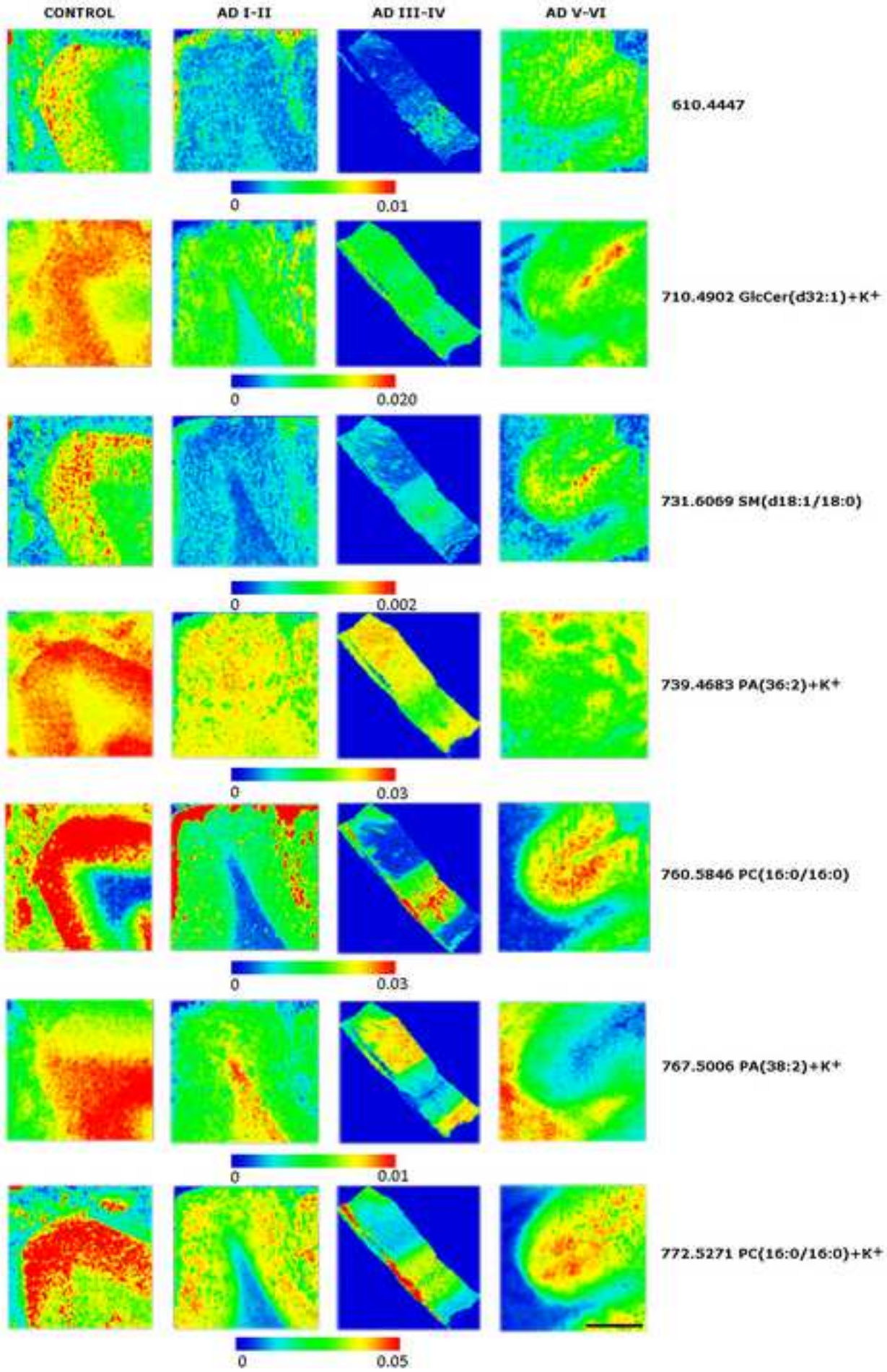

***Conflict of Interest**

Click here to download Conflict of Interest: Package2.pdf